

Face Forgery Detection with Elaborate Backbone

Zonghui Guo, *Member, IEEE*, Yingjie Liu, *Student Member, IEEE*, Jie Zhang, *Member, IEEE*, Haiyong Zheng, *Senior Member, IEEE*, and Shiguang Shan, *Fellow, IEEE*

Abstract—Face Forgery Detection (FFD), or Deepfake detection, aims to determine whether a digital face is real or fake. Due to different face synthesis algorithms with diverse forgery patterns, FFD models often overfit specific patterns in training datasets, resulting in poor generalization to other unseen forgeries. This severe challenge requires FFD models to possess strong capabilities in representing complex facial features and extracting subtle forgery cues. Although previous FFD models directly employ existing backbones to represent and extract facial forgery cues, the critical role of backbones is often overlooked, particularly as their knowledge and capabilities are insufficient to address FFD challenges, inevitably limiting generalization. Therefore, it is essential to integrate the backbone pre-training configurations and seek practical solutions by revisiting the complete FFD workflow, from backbone *pre-training* and *fine-tuning* to *inference* of discriminant results. Specifically, we analyze the crucial contributions of backbones with different configurations in FFD task and propose leveraging the ViT network with self-supervised learning on real-face datasets to pre-train a backbone, equipping it with superior facial representation capabilities. We then build a competitive backbone fine-tuning framework that strengthens the backbone’s ability to extract diverse forgery cues within a competitive learning mechanism. Moreover, we devise a threshold optimization mechanism that utilizes prediction confidence to improve the inference reliability. Comprehensive experiments demonstrate that our FFD model with the elaborate backbone achieves excellent performance in FFD and extra face-related tasks, *i.e.*, presentation attack detection. Code and models are available at <https://github.com/zhenglab/FFDBackbone>.

Index Terms—Face forgery detection, Deepfake detection, presentation attack detection, Vision Transformer, self-supervised learning.



1 INTRODUCTION

HUMAN faces, being unique and readily available biometric data, play a pivotal role in various research fields, including face recognition [1, 2], generation [3, 4], and analysis [5, 6]. Unfortunately, facial information leakage and theft have spawned a clandestine industry where criminals exploit forged faces to perpetrate illegal activities, posing an extreme threat to national security, social stability, and individual well-being. Meanwhile, diverse GAN-based and Diffusion Model-based methods [7–9] in Artificial Intelligence Generated Content (AIGC) have drastically reduced the barriers to creating lifelike forged faces. The proliferation of these forged faces online has led to significant crises in the security and authenticity of information. Therefore, distinguishing digitally forged faces created by image/video synthesis algorithms, *i.e.*, *Face Forgery Detection* (FFD), also referred to as Deepfake detection, has become a critical issue in both research and industrial communities [10–12].

Due to the diverse forgery patterns induced by different types of synthesis algorithms (*e.g.*, entire face synthesis [13], face swapping [14], face attribute editing [15], and face

reenactment [16]), FFD models often overfit specific forgery patterns within training datasets while neglecting implicit forgery cues shared across datasets, severely limiting their generalization. Unlike general image classification tasks that mainly concentrate on salient objects, FFD is a weak signal detection and classification task, where the increasing realism of forged faces obscures forgery cues behind complex facial features, making it more challenging for FFD models to uncover implicit forgery cues. Consequently, FFD models with better generalization must excel in two critical capabilities: robust facial feature representation and precise weak-forgery-cue extraction. Notably, both critical capabilities essentially stem from *pre-training* and *fine-tuning* of the backbone as a foundational model, which is a rational paradigm for improving generalization and achieving remarkable performance in various CV and NLP tasks. However, previous FFD methods often overlook the backbone’s capabilities, leading to unsatisfactory generalization.

Indeed, previous FFD methods also employ existing backbones as a fundamental unit in their models and propose various fine-tuning techniques to equip the backbone for better generalization. However, these backbones are typically used directly without adequate attention, especially regarding the compatible relationship between their differing capabilities and FFD challenges. Furthermore, we are surprised that most backbones used in FFD models are CNN-based [17–20] rather than Transformer-based [21] networks, all of which are pre-trained with supervised learning (SL) on ImageNet for general scene tasks such as natural image classification and recognition. In contrast, backbones with self-supervised learning (SSL) and Transformer-based

- Zonghui Guo is with the Key Laboratory of AI Safety of CAS, Institute of Computing Technology, Chinese Academy of Sciences (CAS), Beijing 100190, China. E-mail: guozonghui@ict.ac.cn.
- Jie Zhang, and Shiguang Shan are with the Key Laboratory of AI Safety of CAS, Institute of Computing Technology, Chinese Academy of Sciences (CAS), Beijing 100190, China, and the University of Chinese Academy of Sciences, Beijing 100049, China. E-mails: {zhangjie, sgshan}@ict.ac.cn.
- Yingjie Liu and Haiyong Zheng are with the College of Electronic Engineering, Ocean University of China, Qingdao 266404, China. E-mails: yingjieliu@stu.ouc.edu.cn, zhenghaiyong@ouc.edu.cn.
- Shiguang Shan is the corresponding author.

Manuscript received April 19, 2005; revised August 26, 2015.

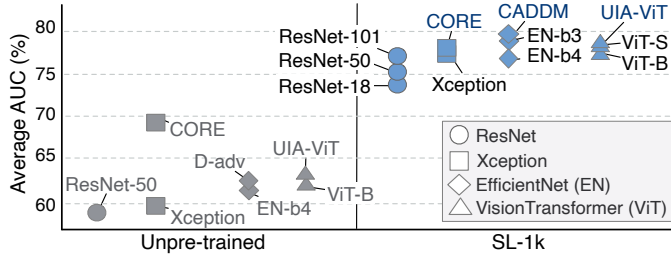


Fig. 1. Quantitative comparison of FFD methods with various backbones. “Unpre-trained” means networks with randomly initialized parameters, while “SL-1K” denotes those pre-trained with supervised learning on ImageNet-1K. The average AUC across three cross-datasets (CelebDF, DFDC, and FFIW) better reflects the generalization of FFD models.

networks have proven superior feature representation capabilities in numerous CV tasks [22, 23], with their importance also highlighted by foundation models like MAE [24], BEiT [25, 26], CLIP [27], and GPT [28]. We reason that different backbone configurations can significantly influence the sensitivity of FFD models to subtle anomalous signals.

Technically, we employ a lightweight fine-tuning structure that directly reflects the backbone’s capabilities, *i.e.*, *Backbone and FC with Cross-entropy loss*, and conduct experiments by replacing backbones used in most FFD methods, such as ResNet [29], Xception [30], EfficientNet [31], and ViT [32]. As shown in Figure 1, the overall comparison results indicate that different backbones lead to substantial variations in performance. Notably, (1) backbones with randomly initialized parameters typically exhibit poor performance and may even fail to converge (**Unpre-trained**); (2) existing FFD methods’ performance primarily stems from the backbones (**SL-1k**), with CORE [33] based on Xception showing similar performance to Xception alone, CADDM [18] and EfficientNet-b3 performing similarly, as do Uia-ViT [21] and ViT-B (Average AUC↑: 77.97 vs. 77.11); (3) ViT and EfficientNet perform comparably, suggesting that supervised pre-training on ImageNet might not fully activate the potential of Transformers in FFD task. Therefore, there is a critical demand to integrate backbone pre-training configurations into FFD solutions and revisit FFD within its complete workflow, from backbone *pre-training* and *fine-tuning* to *inference* of final discriminative results.

It is well known that developing a highly generalized backbone necessitates massive datasets as the knowledge source, high-capacity networks as the carrier, and promising training methods as the drivers. *For the datasets*, facial images exhibit significant deviations from generic natural images (*e.g.*, ImageNet) due to their unique inherent characteristics, including specific shapes, key point distributions, and locally consistent displacement fields [34, 35]. However, most backbones used in FFD models are pre-trained on ImageNet, which insufficiently represents fine-grained facial features. Indeed, in order to recognize real faces and capture their subtle differences from forged faces, a sophisticated FFD backbone may need three levels of knowledge: the general knowledge of image representation from large-scale natural images, the specific knowledge of facial representation from real faces, and the expert knowledge of identifying forgery cues from forged faces. *For the networks*, as shown in

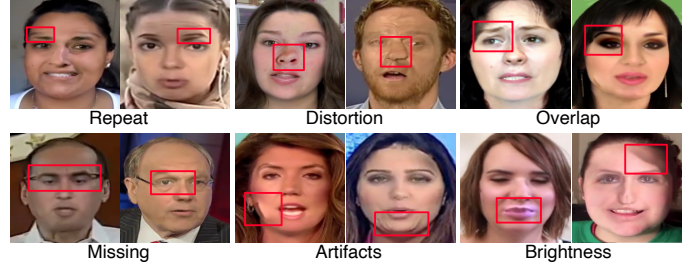


Fig. 2. Representative forged face examples with forgery cues primarily in facial components such as eyebrows, nose, eyes, and lips.

Figure 2, forgery clues often appear in local regions and their global differences within the face, requiring the networks to carry extensive facial knowledge and better capture long-range correlations and differences. *For the training methods*, as the core bridges that assemble knowledge onto the carrier, their pre-training and fine-tuning methods must closely match facial characteristics and FFD challenges, especially in exploring implicit forgery cues within facial components (*e.g.*, eyebrows, eyes, and lips). Building upon this, we strive to develop an elaborate FFD backbone by delving into the correspondent relationship between the backbone’s capabilities and FFD problems.

Given that the final performance of FFD methods heavily depends on backbones, equipping the elaborate backbone with general, specific, and expert knowledge in the *pre-training* and *fine-tuning* stages is a rational and promising solution to enhancing the generalization of FFD models. Moreover, FFD’s ultimate goal is to determine whether the input face is real or fake, but FFD models usually output continuous prediction probabilities ($p \in [0, 1]$) obtained through the *Softmax* function. Existing works empirically use 0.5 as the threshold, converting continuous probabilities into discrete results (real or fake). However, it is hard to say that 0.5 is the optimal threshold, as it varies significantly across different datasets and FFD models, and *Softmax* often produces overconfident prediction scores, which can lead to severe consequences in cases of overconfident incorrect predictions [36, 37]. Therefore, we seek a threshold optimization mechanism by integrating prediction probability and its confidence during the *inference* stage, further improving the backbone’s reliability and practicality.

In addition to digitally forged faces, a category of fake faces made with physical materials, such as printed photos, replayed images/videos, and 3D masks, which also pose a significant threat in real-life scenarios, particularly the attacks on face recognition systems. Research on detecting these attacks, known as presentation attack detection [38–40] (PAD), face anti-spoofing [41–47], and face liveness detection [48–50], has also garnered widespread attention [51]. Since FFD and PAD are both binary classification tasks for distinguishing real or fake faces, we consider that the backbones can still play an essential role in PAD. Therefore, we further apply our FFD method to PAD to validate its potential and broaden its applicability.

In summary, the main contributions of this work are as follows: (1) we propose a revitalized FFD pipeline through a complete revisiting from backbone *pre-training* and *fine-tuning* to *inference* of discriminant results; (2) we develop

and pre-train a proficient backbone that better represents facial component features tailored for FFD task; (3) we build a competitive backbone fine-tuning framework to enhance the backbone’s capabilities in extracting diverse forgery cues; (4) we devise a threshold optimization mechanism to improve the backbone’s accuracy and reliability in inference results; (5) we conduct extensive experiments to demonstrate the superiority and potential of our elaborate backbone, achieving significantly better generalization than previous methods in FFD and extra face-related PAD tasks.

2 RELATED WORK

Our work strives to seek insightful guidance and practical solutions by comprehensively revisiting FFD workflow and analyzing the critical role of backbones with different pre-training configurations in FFD task. We start by summarizing existing FFD methods and then describe supervised and self-supervised learning, both of which enhance the feature representation capabilities of backbones.

2.1 Face Forgery Detection

Thanks to the creation of numerous face forgery datasets such as FaceForensic++ [52], Celeb-DF [53], and DFDC [54], deep learning-based FFD methods have made considerable advancements and can achieve outstanding accuracy within training datasets (exceeding 95%). However, their performance drops sharply when encountering unseen forgery patterns across different datasets. Recent FFD work aims to improve model generalization by implementing specific fine-tuning methods such as data augmentation [20, 55–57], attention mechanisms [21, 58–63], forgery feature decoupling [17, 64–71], and temporal inconsistency [19, 57, 72, 73], as well as spatial and frequency fusion [74–76].

Data augmentation enlarges the diversity of training data via various image transformations, which becomes a common setting in the training stage, especially for domain generalization tasks. Face X-ray [56] proposed an augmentation method for generating forgery faces and boundaries by fusing source face images with similar faces obtained through nearest neighbor search. Chen *et al.* [77] proposed a synthesized forgery face method from two real face images by adjusting forgery configurations, such as forgery region, blending type, and blending ratio. SBI [55] built a source-target generator to generate pseudo-source and target images through different image transformations, combined with blending masks to produce forged faces. LSDA [20] enriched the diversity of forged samples by fusing and transforming features of different forgery types in the latent space to learn more generalized decision boundaries.

Attention mechanisms, known for their ability to focus on task-relevant critical features, have been widely applied in most computer vision tasks. Many FFD methods also incorporate diverse attention networks into the middle or later layers of the backbone to assist in identifying forgery clues or localizing forged regions within faces [21, 58–63]. Some methods utilized convolutional or linear transformations for adaptive learning and estimating attention maps of forged regions [58, 61], while others employed attention maps to erase conspicuous and specific forgery traces

within the training dataset, compelling the detection model further to explore generic forgery features [59, 60]. Subsequently, attention mechanisms have become increasingly sophisticated. Fei *et al.* [62] proposed a second-order local anomaly learning module to mine local region anomalies by calculating fine-grained local anomalies of the first and second order. Sun *et al.* [63] found that face forgery is closely associated with high-information content and designed the Self-Information Attention to utilize self-information as a theoretical guide for capturing forgery cues while highlighting more informative regions. Zhuang *et al.* [21] proposed an Unsupervised Inconsistency-Aware method based on Vision Transformer, *i.e.*, UIA-ViT, to extract inconsistency cues without pixel-level forged location annotations.

Due to the presence of redundant forgery-independent features in forged faces (*e.g.*, identity, natural artifacts), the distinction of forgery-dependent features is disrupted and hindered. Researchers leveraged disentangled representation learning [78] or game-theoretical approaches to enhance the backbone’s ability for extracting forgery clues. Specifically, disentangled representation learning-based FFD methods primarily adopted a training process that involved exchanging decoupled forgery-independent and forgery-dependent features to reconstruct pairs between real and forged faces, enhancing the discriminative performance of the classification branch with the backbone encoder [17, 64–69]. Game-theoretical-based FFD methods [79, 80] utilized the knowledge of game theory to decouple unrelated regions from source and target images, promoting FFD performance with the support of Shapley value [81].

FTCN [72] and AltFreezing [57] explored temporal inconsistencies in forged videos. FTCN reduced the spatial convolution kernel, while AltFreezing alternated between spatial and temporal freezing, both aiming to encourage ResNet3D to explore generic features of forged face videos. Choi *et al.* [19] employed StyleGRU and a style attention module to exploit the temporal low-variance properties of style latent vectors in each frame for detecting forged videos. Additionally, Wang *et al.* [74] and Miao *et al.* [75] leveraged frequency domain information to assist the backbone in capturing more fine-grained artifact features.

After reviewing previous FFD methods and their technical implementations, we find that these methods consistently equip various fine-tuning techniques to backbones, such as ResNet [29], Xception [30], EfficientNet [31], and ViT [32], which are pre-trained with supervised learning on ImageNet. These backbones are often used directly in the *fine-tuning* stage while overlooking the crucial roles of both the *pre-training* and *inference* stages, as shown in Figure 4(top). In contrast, we endeavor to offer comprehensive research insights and guidance for FFD generalization by revisiting the complete FFD workflow.

2.2 Supervised and Self-Supervised Learning

Early backbone research utilized supervised learning (SL) with an image classification task as the pre-training approach, focusing on designing more sophisticated network architectures to improve backbone capacity and capability. During this period, numerous well-designed networks developed for the ImageNet Large-Scale Visual Recognition Challenge [82] demonstrated outstanding performance,

such as GoogLeNet [83], VGG [84], ResNet [29], and SENet [85]. Benefiting from Transformers’ global contextual attention design, backbone network architectures have gradually transitioned from CNNs to Transformers. In particular, Vision Transformers (ViTs) [32] have come to dominate the field of computer vision (CV), achieving superior performance compared to ResNet, Xception, and EfficientNet.

Since SL with the classification pretext task relies on annotated datasets, it somewhat restricts the capability of pre-trained backbones. Recent research on backbones has gradually shifted from SL to self-supervised learning (SSL) [22, 86], which can flexibly employ different pretext tasks and larger-scale training datasets without annotations. SSL has significantly improved backbones’ feature representation capabilities, surpassing SL methods [29, 32] in most CV tasks. SSL is usually divided into discriminative and generative approaches based on different technical implementations and pretext tasks. With technological advancements, contrastive learning (CL) and masked image modeling (MIM) have gradually become the mainstream discriminative and generative SSL paradigms, respectively.

Discriminative SSL typically ensures representation consistency across different augmented views of the same image using Siamese architectures, which can be divided into clustering, CL, distillation, and information maximization. Clustering SSL methods, such as Deep Cluster [87], SCAN [88], and Swav [89], are among the early SSL methods and used techniques like K-Means, advanced neighbor search, and contrastive elements. CL methods, such as MoCo [90–92] and SimCLR [93, 94], achieved instance discrimination by pulling positive samples closer in the latent space while pushing negative samples further apart. Distillation SSL methods, such as BYOL [95], SimSiam [96], and DINO [97], trained a student network to predict the outputs of a teacher network, preventing collapse into identical representations and eliminating the need for negative samples. VICReg [98] is an information maximization SSL method that eliminates correlations between different samples in the feature space to learn independent features.

The success of autoregressive modeling in GPT [28] and masked autoencoding in BERT [99] for NLP has driven the development of generative SSL with MIM in computer vision. The MIM approach involves masking part of the input image and training the backbone to predict the missing content. Based on different pretext tasks, MIM can be divided into predicting pixel values (e.g., MAE [24] and SimMIM [23]) and predicting discrete visual tokens (e.g., BEiT [25, 26, 100] and CAE [101]).

Given the significance of learning approaches with different pretext tasks for backbones in the *pre-training* stage, we conduct a comprehensive empirical study to evaluate their performance in FFD task and provide valuable guidelines for their selection and optimization.

3 FFD WORKFLOW AND METHOD

3.1 Research Overview

With the continuous expansion of massive data and computational resources, deep learning-based works increasingly follow the three-stage pipeline of *pre-training*, *fine-tuning*,

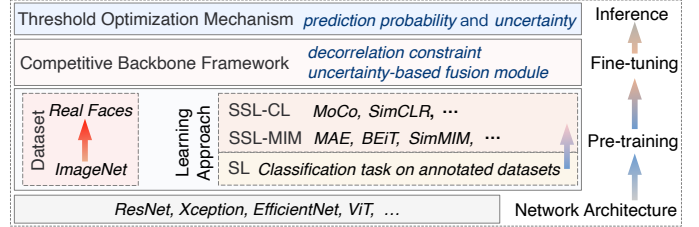


Fig. 3. Overview of our research to revisit the complete FFD workflow from backbone *pre-training* and *fine-tuning* to *inference* in discriminant results. This includes network architectures, datasets, learning approaches with supervised learning (SL) and self-supervised learning (SSL), which encompass contrastive learning (CL) and masked image modeling (MIM) pretext tasks, as well as our competitive backbone fine-tuning framework and threshold optimization mechanism.

and *inference*. As a typical binary classification task, we consider that the build process of FFD models also adheres to this pipeline, although these existing works primarily focus on optimizing fine-tuning techniques. Therefore, we aim to revisit the FFD workflow from backbone development to final applications and further develop a practical and reliable backbone for FFD task, which ultimately determines whether an input face is real or fake.

Backbone serves as the starting point and foundation of FFD workflow, and following our investigation of backbones with different pre-training configurations, we construct a comprehensive research overview, as shown in Figure 3. This overview covers the complete FFD workflow: (1) the network architectures, (2) the learning approaches with SL and SSL, as well as the datasets such as ImageNet and real faces during *pre-training*, (3) the adaptation methods to downstream tasks during *fine-tuning*, and (4) the application mechanisms to maximize performance during *inference*.

Specifically, we explore the critical role of backbones with different configurations in FFD task and seek insightful solutions that align with FFD challenges during the *pre-training* stage (Section 3.2). We then introduce our backbone fine-tuning framework with a decorrelation constraint and an uncertainty-based fusion module, which improves the backbone’s ability to extract forgery cues during the *fine-tuning* stage (Section 3.3). Moreover, we analyze the limitations of FFD methods in discriminant results and propose a threshold optimization mechanism by integrating prediction probability and confidence to enhance the practicality of FFD models during the *inference* stage (Section 3.4).

3.2 FFD with Pre-trained Backbones

We abstract a traditional pipeline of existing FFD methods to highlight the vital role of backbones, as shown in Figure 4(top). These methods directly use backbones pre-trained with SL on ImageNet, implement fine-tuning networks or strategies to equip the backbone for better generalization, and apply an empirical classification threshold (0.5) to output the final discriminant result (real or fake).

Relying on our research overview, we first explore the impact of pre-training backbones with different network architectures and learning approaches in FFD task. Technically, we utilize a basic fine-tuning structure (*Backbone and FC with Cross-entropy loss*) and prioritizing various mainstream backbones pre-trained on ImageNet to evaluate FFD

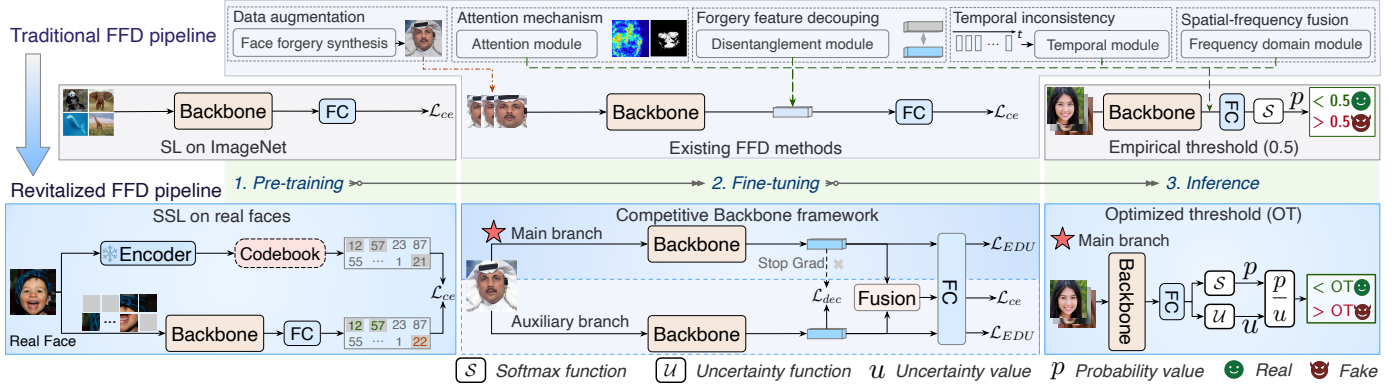


Fig. 4. FFD workflow evolves from the traditional pipeline to our revitalized FFD pipeline. Existing FFD methods primarily rely on backbones pre-trained with supervised learning on ImageNet, applying various techniques during *fine-tuning*, and using empirical classification thresholds during *inference*. In contrast, our FFD pipeline offers a more proficient, promising, and reliable solution by incorporating self-supervised learning on real faces, a competitive backbone framework, and an uncertainty-based threshold optimization mechanism across the three stages.

performance. Meanwhile, we select CNN-based architectures such as ResNet, Xception, and EfficientNet, which are common in previous FFD methods, as well as Transformer-based architectures like ViT, which are superior in most other CV tasks. For learning approaches, we employ SL and SSL with different pretext tasks, including contrastive learning (CL) tasks such as SimSiam [96] and MoCo [90, 91], as well as masked image modeling (MIM) tasks such as MAE [24], BEiT [25, 26], and ConMIM [102].

In our comprehensive comparison (refer to Section 4.2), we statistically find that backbones pre-trained with SSL outperform those with SL under the same network architecture, and Transformer-based backbones outperform CNN-based ones with the same learning approach. These results are consistent with recent research trends observed across various tasks. Notably, BEiT [25, 26] achieves superior performance, benefiting from its ability to independently represent visual tokens of image patches, thus better extracting differential cues between facial local components.

Since most mainstream backbones are pre-trained on ImageNet, which contains content significantly different from facial images, this training data gap will also restrict the performance of general-purpose backbones in facial-related tasks, particularly FFD, which requires identifying subtle forgery cues within complex facial features. Furthermore, compared to forgery faces, we can easily collect large-scale and diverse real-face datasets [103, 104]. Although these datasets may lack labels, we can still leverage SSL with appropriate pretext tasks to pre-train a robust face representation backbone with face-specific knowledge tailored to facial tasks. In the technical implementation of the backbone, we adopt ViT as the network architecture and employ SSL methods such as MoCo v3 [90], MAE [24], and BEiT v2 [25], which are concise and classical in CL and MIM.

As expected, the backbone pre-trained on real-face datasets yields superior FFD generalization compared to one on ImageNet, as evident in *SSL-Face* and *SSL-1k&Face* of Table 1. Notably, MoCo v3 and BEiT v2 are superior to MAE, whose performance is relatively weaker. We attribute these results to the close relationship between FFD core challenges and the backbone’s pretext tasks. On the one hand, forgery clues typically manifest in the local components of fake

faces (e.g., eyebrows, eyes, lips) and the contrast between facial components, as depicted in Figure 2. On the other hand, MoCo v3, with its CL pretext task that compares the similarity of high-level features from differently augmented images, can better focus on forgery cues in local regions between these images. Meanwhile, with a classification pretext task based on encoding image patches, BEiT v2 excels at discerning the authenticity of local facial components. The excellent performance of MoCo v3 and BEiT v2 further demonstrates the indispensability of equipping backbones with both general and specific knowledge through appropriate pre-training methods to enhance FFD generalization.

Based on our comprehensive study of backbones in the *pre-training* stage, we revitalize the traditional FFD pipeline by integrating SSL on real-face datasets, a competitive backbone framework, and an uncertainty-based threshold optimization mechanism in the *pre-training*, *fine-tuning*, and *inference* stages. As shown in Figure 4(bottom), our revitalized FFD pipeline enables a more proficient and promising step-by-step enhancement of the backbone’s baseline and task-specific capabilities, as well as greater reliability in FFD discriminant results. Additionally, given the superior performance of BEiT v2, we use its SSL method and ViT architecture as the representative pre-training configuration in our pipeline, as shown in Figure 4(left-bottom). Next, we introduce our competitive backbone fine-tuning framework.

3.3 Competitive Backbone Fine-tuning Framework

Although the backbone pre-trained on real-face datasets better represents facial features, employing promising fine-tuning methods to equip the backbone with expert knowledge from forgery faces remains crucial for FFD. Hence, we further analyze the inherent characteristics of FFD problem. Humans often identify forged faces by noticing semantic repetition or inconsistencies in facial components and contrast in appearance between them, as illustrated in Figure 2. Correspondingly, the apparent and implicit forgery cues in the latent space of forged faces are even more diverse and entangled, making it nearly impossible to explicitly disentangle these two types of cues due to the lack of available definitive constraints. Therefore, we consider leveraging

two backbones to competitively mine different forgery cues in the latent space to enhance generalization.

Inspired by MoCo v3 with a dual-branch Siamese architecture, where the pre-trained backbone effectively extracts facial component features and achieves excellent FFD performance, we propose building a dual-branch framework that cultivates two backbones to extract different forgery cues within a competitive adversarial learning mechanism. However, MoCo v3 primarily constrains the backbones to represent the semantic similarity of two differently augmented images, which involve changes in both high-level (e.g., crop, resize) and low-level (e.g., color distortion, Gaussian blur) features. These different augmentations of the same image may potentially lead to the loss or introduction of subtle forgery traces related to low-level features, such as artifacts and appearance. Thus, we remove the image augmentations and contrastive loss while retaining only the dual-branch architecture and incorporating cross-entropy loss \mathcal{L}_{ce} for FFD. Furthermore, we fuse the output features of both backbones to enable their interaction, thereby forming our basic dual-branch backbone fine-tuning architecture.

Since the dual branches have the same inputs (without different augmented images) and loss functions (\mathcal{L}_{ce}), the features extracted by both backbones will inevitably be similar. Thus, this basic dual-branch architecture alone cannot make both backbones competitively learn different forgery cues. To address this, we introduce a feature metric as a decorrelation constraint to minimize the correlation between features extracted by both backbones, enabling competitive learning within the dual-branch architecture.

Decorrelation Constraint. We employ the Pearson correlation coefficient as the decorrelation constraint \mathcal{L}_{dec} to measure and minimize the linear correlation between class tokens of the dual-branch backbones. Under the combined constraints of \mathcal{L}_{dec} and \mathcal{L}_{ce} on the dual branches, both backbones achieve competitive learning of different forgery cues. Moreover, we utilize a gradient-stopping backpropagation strategy on one branch under the constraint of \mathcal{L}_{dec} to particularly foster the forgery cue extraction capability of that branch’s backbone, while enabling both backbones to compete in the fusion module for their contributions to this task. Additionally, we refer to the fostered branch as the **main** branch and the other as the **auxiliary** branch.

At this point, the dual-branch architecture with decorrelation constraint is preliminarily established, as shown in Figure 4(middle-bottom), namely *competitive backbone fine-tuning framework*. It includes two unshared backbones processing the same face image, feature fusion module, and three \mathcal{L}_{ce} , which constrain both backbones to competitively mine different forgery cues to enhance the main branch’s generalization. \mathcal{L}_{dec} and \mathcal{L}_{ce} are defined as follows:

$$\mathcal{L}_{dec} = \frac{\sum_{i=1}^C (f_M^i - \bar{f}_M)(f_A^i - \bar{f}_A)}{\sqrt{\sum_{i=1}^C (f_M^i - \bar{f}_M)^2 \sum_{i=1}^C (f_A^i - \bar{f}_A)^2}}, \quad (1)$$

$$\mathcal{L}_{ce} = -(y \log(p) + (1 - y) \log(1 - p)), \quad (2)$$

where f represents the feature vectors from both main (M) and auxiliary (A) backbones with dimensions C , while y and p are the label and predicted probability, respectively.

Uncertainty-based Fusion Module. Indeed, directly summing the feature vectors of both backbones implies

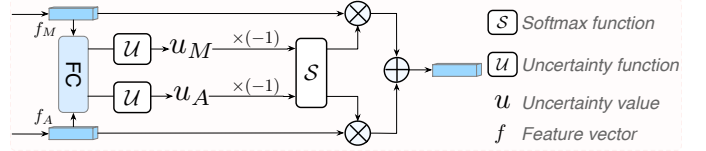


Fig. 5. Our uncertainty-based fusion module, calculates uncertainty using features from the main (M) and auxiliary (A) branches, then inputs these into *Softmax* to obtain weights for fusing the features as output.

equal contribution, which will limit their competition in a naive fusion operation. To stimulate the competitive detection of forgery cues by both backbones, we further explore assigning different fusion weights to each branch based on the confidence of their discrimination results, dynamically giving greater weight to the more confident branch.

Standard classification networks typically use *Softmax* in their final layer to convert the continuous output values into class probabilities. However, *Softmax* tends to exaggerate the probabilities of predicted classes due to its exponential function, which cannot accurately reflect the model’s prediction confidence. Despite minimizing the \mathcal{L}_{ce} of predicted classes during training, the classification model lacks awareness of its prediction confidence. To overcome this issue, uncertainty estimation methods have been proposed to assess the model’s confidence in its predictions [37]. Particularly, Evidence Deep Learning (EDL) simultaneously predicts a model’s class probability and its uncertainty by assuming that the predicted class probabilities follow a prior Dirichlet distribution [105–107]. Therefore, we utilize the uncertainties (u) from both branches as weights (w) to fuse their feature vectors, as shown in Figure 5, enabling flexible and dynamic competition between both backbones. The fusion process is as follows:

$$S = \sum_{k=1}^K (e_k + 1), \text{ where } e = \sigma(\Phi(f)), \quad (3)$$

$$w_M, w_A = \text{softmax}(-u_M, -u_A), \text{ where } u = K/S, \quad (4)$$

$$F = w_M f_M + w_A f_A, \quad (5)$$

where Φ denotes the classification header (e.g., FC), σ is a non-negative evidence function ensuring that evidence $e \geq 0$ (e.g., \exp , ReLU), and K denotes the total number of classes, i.e., $K = 2$ in FFD task.

Furthermore, we employ EDL and Evidential Uncertainty Calibration (EUC) losses [106] to improve the accuracy of predicted probability and uncertainty, as follows:

$$\mathcal{L}_{EDL} = \sum_{k=1}^K y_k (\log S - \log(e_k + 1)), \quad (6)$$

$$\mathcal{L}_{EUC} = -\lambda_t \sum_{i \in \{\hat{y}=y\}} p \log(1 - u) \quad (7)$$

$$- (1 - \lambda_t) \sum_{i \in \{\hat{y} \neq y\}} (1 - p) \log(u), \quad (8)$$

where y denotes a one-hot K -dimensional label, \hat{y} represents the class with the highest probability p for the input image, and p is calculated as $p = \max((e_k + 1)/S)$. Additionally, the annealing factor λ_t is defined as $\lambda_t = \lambda_0 \exp\{-(\ln \lambda_0/T)t\}$, where t and T denote the current training epoch and the total number of training epochs, respectively. For further details, please refer to Bao *et al.*[106].

As shown in Figure 4(middle-bottom), we replace the \mathcal{L}_{ce} with \mathcal{L}_{EDL} and \mathcal{L}_{EUC} in both the main and auxiliary branches. Thus, the loss function \mathcal{L} of our competitive backbone fine-tuning framework for FFD task is as follows:

$$\mathcal{L} = \mathcal{L}_{EDU}^M + \mathcal{L}_{EDU}^A + \mathcal{L}_{ce}^F + \mathcal{L}_{dec}, \quad (9)$$

where $\mathcal{L}_{EDU} = \mathcal{L}_{EDL} + \mathcal{L}_{EUC}$.

Thanks to the dedicated design of our decorrelation constraint and uncertainty-based fusion module in our competitive backbone fine-tuning framework, the main backbone is better fostered and significantly enhances its generalization under the stimulation of the auxiliary backbone. Consequently, only the main branch is required during *inference*, also saving half of the computational resources.

3.4 FFD Inference with Optimized Threshold

In academic research, FFD models' performance is typically evaluated using the Area Under the Receiver Operating Characteristic Curve (AUC), which measures overall results across a dataset with thresholds sampled at fixed intervals without needing explicit real or fake outputs [108]. However, in practical FFD applications, a threshold τ is required as an anchor value to classify the FFD model's continuous probability outputs ($p \in [0, 1]$) into discrete results, such as $p \geq \tau$ indicates fake and $p < \tau$ indicates real. This shows that the value of τ is crucial for the classification results, and it also determines the model's performance on evaluation metrics such as ACC, Precision, Recall, and F1-score [109]. However, most FFD works empirically set $\tau = 0.5$, it is usually not optimal, as each model's optimal threshold is different and depends on various factors such as its architecture, training approach, and dataset.

Due to the overfitting performance of FFD models within the training dataset, their predicted probabilities p are typically polarized, with real being $p \approx 0$ and fake being $p \approx 1$. In such cases, τ has little impact on within-dataset accuracy. However, given the diverse forgery cues across different cross-datasets, where p values are more evenly distributed, this leads to τ becoming highly sensitive for FFD model prediction accuracy. Therefore, we strive for a threshold selection mechanism by selecting the optimal threshold τ_{ot} on one cross-dataset and validating its efficacy on others.

Specifically, we iterate through the predicted probabilities of all faces in one cross-dataset, treating each probability as a potential threshold and calculating the corresponding ACC for the dataset. The threshold with the highest ACC is determined to be τ_{ot} . The calculation of τ_{ot} is as follows:

$$\tau_{ot} = \arg \max_{\tau} \text{ACC}(\tau), \quad (10)$$

$$\text{ACC}(\tau) = \frac{1}{N} \sum_{i=1}^N [\mathbb{I}(p_i \geq \tau)y_i + \mathbb{I}(p_i < \tau)(1 - y_i)], \quad (11)$$

where N is the total number of face images, y_i is the label for the i -th image (with 1 for fake and 0 for real), and \mathbb{I} is the indicator function returning 1 if true and 0 otherwise.

Note that the method above for finding the τ_{ot} resembles a white-box scenario. When the predicted probabilities of all images are unknown but the overall ACC is available, we can still approximate the optimal threshold by searching over $\tau \in [0, 1]$ with a defined step size. Moreover, the

comparison of $\tau = 0.5$ and $\tau = \tau_{ot}$ in Table 8 indicates that τ_{ot} from one cross-dataset can significantly improve the ACC of other datasets, underscoring the critical role of optimized thresholds in FFD applications.

As mentioned in the Uncertainty-based Fusion Module of Section 3.3, the class probabilities amplified by *Softmax* can cause the model to be overly confident in its predictions, even when it is wrong. To mitigate this, we propose introducing the uncertainty u to adjust the probability p , which is crucial for improving the reliability of the predictions. Moreover, we devise a threshold optimization mechanism where dividing p by u yields the adjusted probability p' , i.e., $p' = p/u$, which enhances p with high confidence (low uncertainty) and reduces p with low confidence (high uncertainty), as shown in Figure 4(right-bottom). Based on the adjusted probability p' , we recompute the optimal threshold using Equations 10 and 11 to improve the reliability of FFD models in final discriminant results. For more comparisons, please refer to Section 4.5.

4 EXPERIMENT

4.1 Experimental Setup

4.1.1 Datasets

We conduct experiments by *pre-training* on real-face dataset, *fine-tuning* on c23 of Faceforensics++ [52] (FF++), and evaluating on multiple cross-datasets during *inference*. Specifically, our real-face dataset contains 550,000 images from CelebA [103], CelebV-Text [110], and FFHQ [104]. FF++ contains 1,000 real videos and 4,000 manipulated videos obtained by four forging methods: DeepFakes [111], FaceSwap [112], Face2Face [113], and NeuralTexture [114]. Cross-datasets consist of Celeb-DF [53] (CDF), DFDC [54], and FFIW [115]. CDF includes real videos of 59 celebrities from YouTube and fakes generated via an improved synthesis process [53]. DFDC is a large-scale face-changing video dataset, created using various Deepfake and GAN-based methods, with a total of 5,000 test videos. FFIW is a challenging multi-face forgery dataset with 10,000 videos.

To comprehensively evaluate the generalization of FFD models, we construct 9 new cross-datasets generated by various mainstream GAN-based methods (e.g., DCGAN [116], StyleGAN3 [13], StarGAN2 [15], AttnGAN [117], E4S [14], and Wav2Lip [16]) and Diffusion Model-based methods (e.g., SD-1.5 [118], DiffFace [119], and Diffused Heads [120]), with the forged faces covering four types of forgeries: entire face synthesis, face attribute editing, face swapping, and face reenactment. Each cross-dataset consists of 5,000 real faces and 5,000 forged faces from each method.

4.1.2 Implementation Details

Following MoCo v3, MAE, and BEiT v2 settings, we pre-train ViT on our real-face dataset using 4x A100 GPUs until full convergence. We use RetinaFace [121] for face cropping, resize the cropped faces to 224×224, and sample 8 frames at equal intervals from each video. Fine-tuning is performed on 2x GTX 3090 GPUs with a batch size 64, using the Lamb optimizer [122] and a learning rate $5e - 5$ with cosine decay for 60 epochs. Notably, backbones pre-trained on real faces with more robust facial feature representation capabilities converge in just 10 epochs.

4.1.3 Evaluation Metrics and Protocols

Evaluation Metrics. Following many existing FFD and PAD works, we use the Area Under the Receiver Operating Characteristic Curve (AUC) and Half Total Error Rate (HTER) as evaluation metrics, respectively. Video-level scores are computed by averaging frame-level scores for comparison.

Evaluation Protocols. Existing FFD works typically evaluate the model’s generalization performance on unseen cross-datasets, such as training on FF++ and evaluating on CDF, DFDC, and FFIW. In real-world scenarios, it is possible to obtain a small number of images from unseen datasets. Further fine-tuning the FFD model with these few images can better demonstrate its adaptability, as a highly adaptable model can effectively counter emerging forgery algorithms while providing significant real-world utility. Therefore, we evaluate the FFD model’s practicality and robustness using two protocols: generalization and adaptation.

4.2 Comparison of FFD with Pre-trained Backbones

We conduct experiments to evaluate FFD performance of backbones with various learning approaches, network architectures, and datasets. The quantitative evaluation results are shown in Table 1. We use the backbone with randomly initialized network parameters as a baseline (Unpre-trained) to highlight the importance of pre-training for FFD task.

Unpre-trained Backbones. We utilize unpre-trained backbones with different architectures, including ResNet, Xception, EfficientNet, and ViT, and fine-tune them on FF++ dataset. Their poor AUC results, averaging around 61%, underscore the significance of pre-trained backbones in FFD.

Learning Approaches. We employ mainstream backbones pre-trained with SL and SSL on ImageNet-1K (*i.e.*, *SL-1K* and *SSL-1K*) to evaluate the impact of learning approaches in FFD. As shown in Table 1, *SL-1K* achieves substantially better FFD performance than unpre-trained backbones, demonstrating the indispensability of pre-trained backbones. Furthermore, we use ResNet-50 and ViT-B, commonly used in SSL, as the backbone network architectures. The comparison results in 3.1 and 3.2 of Table 1 indicate that SSL gradually surpasses SL in FFD performance with the improvement of pre-training methods, such as the momentum encoder/contrast in CL equipped in SimSiam, SimCLR, and MoCo, and the MIM pretext task equipped in MAE, BEiT, and ConMIM. This trend is consistent with their performance on downstream ImageNet tasks, proving that appropriate learning approaches are also crucial for FFD.

Network Architectures. We then evaluate the effect of different network architectures, which serve as the backbone’s infrastructure. The comparison results in *SSL-1K* of Table 1 show that the size of the network parameters under the same architecture has little impact on FFD performance. Meanwhile, ViT substantially outperforms ResNet under SSL, *e.g.*, MoCo v3 with ViT-B surpasses ResNet-50 by 3.77% on average AUC across three cross-datasets. Thus, an excellent network architecture combined with an appropriate learning approach will significantly promote the backbone’s baseline performance in FFD.

Pre-training Datasets. We construct a large-scale real-face dataset to pre-train backbones, aiming to enhance their ability to represent facial features by alleviating the gap

TABLE 1

Quantitative comparison of FFD with different backbones. The average AUC (Avg) across three cross-datasets is provided for reference. **1K** and **Face** refer to ImageNet-1K and our real-face dataset, respectively. **1K&Face** denotes a backbone pre-trained on **1K** and then further pre-trained on **Face**. **Bold**, **bold**, and *italics* indicate the best overall, second-best, and best in each section, respectively.

Backbone	In-set	Cross-set AUC↑ (%)			
	FF++	CDF	DFDC	FFIW	Avg
1. Unpre-trained					
ResNet-18 [29]	72.87	58.23	61.53	60.05	59.94
ResNet-50 [29]	75.74	57.86	61.72	59.99	59.86
ResNet-101 [29]	76.54	57.58	63.74	56.84	59.39
Xception [30]	80.18	61.26	63.29	57.41	60.65
EfficientNet-b0 [31]	71.77	54.55	61.61	62.89	59.68
EfficientNet-b3 [31]	73.57	64.14	62.11	66.09	64.11
EfficientNet-b4 [31]	73.07	62.60	57.38	57.73	59.24
ViT-S [32]	70.71	58.41	64.80	54.60	59.27
ViT-B [32]	72.05	61.85	63.61	57.91	61.12
2. SL-1K					
ResNet-18 [29]	97.73	79.09	72.44	71.23	74.25
ResNet-50 [29]	97.95	81.24	72.23	74.21	75.89
ResNet-101 [29]	97.97	82.58	72.16	75.10	76.61
Xception [30]	97.39	82.06	74.05	72.91	76.34
EfficientNet-b0 [31]	97.84	82.77	73.57	76.76	77.70
EfficientNet-b3 [31]	98.35	80.91	74.05	79.08	78.01
EfficientNet-b4 [31]	97.55	81.87	74.42	72.89	76.39
ViT-S [32]	97.61	82.96	77.33	71.14	77.14
ViT-B [32]	97.09	83.39	76.77	71.17	77.11
3.1 SSL-1K (ResNet-50)					
Supervised	97.95	81.24	72.23	74.21	75.89
Obow [123]	98.39	76.38	74.07	78.54	76.33
VicReg [98]	98.20	77.89	72.47	75.47	75.28
BYOL [95]	98.33	81.88	73.72	70.39	75.33
SimSiam [96]	98.53	81.37	73.16	79.26	77.93
SimCLR [93]	98.50	82.08	73.33	77.09	77.50
MoCo v2 [90]	98.37	80.43	73.16	77.49	77.03
MoCo v3 [90]	98.08	84.17	73.64	76.90	78.24
3.2 SSL-1K (ViT-B)					
Supervised	97.09	83.39	76.77	71.17	77.11
Moco V3 [91]	98.29	88.19	79.28	78.56	82.01
MAE [24]	98.31	85.09	76.62	75.96	79.22
BEiT v2 [25]	99.16	89.48	81.00	77.61	82.70
BEiT v3 [26]	98.76	87.99	80.02	80.61	82.87
SimMIM [23]	98.34	84.27	77.29	71.56	77.71
DINO [97]	98.24	84.56	76.77	74.48	78.60
ConMIM [102]	98.40	82.74	78.14	76.09	78.99
3.3 SSL-Face (ViT-B)					
MoCo v3 [91]	98.41	86.30	78.51	83.38	82.73
MAE [24]	98.22	85.43	78.33	80.02	81.26
BEiT v2 [25]	98.93	88.62	80.99	81.71	83.77
3.4 SSL-1K&Face (ViT-B)					
MoCo v3 [91]	98.65	84.98	79.13	85.72	83.28
MAE [24]	98.37	85.85	78.04	78.07	80.65
BEiT v2 [25]	99.14	89.18	84.02	86.48	86.56

between multi-scene images in ImageNet and facial images. We choose the pre-training methods of MoCo v3, MAE, and BEiT v2, which are not only the most representative in CL and MIM but also perform excellently in FFD. We did not use BEiT v3 because its pre-training requires an image-text multimodal dataset. The comparison results in Table 1 indicate that FFD performance of all three methods is superior when pre-trained on the real-face dataset (**3.3 SSL-Face**) compared to ImageNet-1K (**3.2 SSL-1K**), despite the real-face dataset being half the size of ImageNet-1K. Meanwhile, MoCo v3 and BEiT v2 pre-trained on ImageNet-1K achieve more significant improvements when further pre-trained on the real-face dataset (**3.4 SSL-1K&Face**). Remarkably, BEiT v2 improves from 82.70% to 86.56% (Avg AUC↑: **3.2** vs. **3.4**),

proving that its tokenizer classification pretext task better extracts local forgery clues in facial images.

Extensive empirical studies on backbones demonstrate that embedding both general and face-specific knowledge into the network through pre-training methods aligned with FFD challenges is essential for advancing generalization.

4.3 Comparison with State-of-the-arts

We move on to our competitive backbone fine-tuning framework, which enhances the backbone’s forgery detection capabilities through the competitive learning mechanism. We compare our model’s generalization and adaptability with state-of-the-art FFD methods, such as FTCN [72], SBI [55], RECCE [69], CORE [33], UIA-ViT [21], and LSDA [20]. Furthermore, we use BEiT v2 pre-trained on the ImageNet-1K and our real-face dataset as the baseline (BEiT v2’) and introduce SBI to verify its data augmentation performance.

4.3.1 Generalization Evaluation

We first evaluate the generalization capability of various FFD methods on cross-datasets: CDF, DFDC, and FFIW. We also present the average AUC across these three datasets for a clear comparison. Table 2 shows the quantitative comparison results, as can be seen: (1) previous FFD methods exhibit varying and unsatisfactory performance on cross-datasets with diverse forgery patterns, indicating that generalization to unseen cross-datasets remains a significant challenge in FFD task; (2) except SBI [55], which uses sophisticated augmentation strategies instead of FF++ forged videos during training, even our baseline BEiT v2’ significantly outperforms existing methods in generalization, including FTCN [72] and AltFreezing [57], which utilize additional temporal information. These results highlight the significance of a proficient backbone in FFD models, as well as the indispensable role of analyzing the correspondent relationship between the capabilities of different backbones and FFD problems; (3) Ours and Ours+SBI achieve state-of-the-art generalization performance, especially on the more diverse and complex forgery patterns in DFDC and FFIW, which present greater challenges and differ significantly from the within-dataset FF++. These results demonstrate that our competitive backbone fine-tuning framework effectively equips the backbone with a powerful ability to uncover implicit forgery cues across different face synthesis algorithms. Additionally, compared to UIA-ViT [21], which also uses ViT-B as the network architecture, our framework achieves a 10.81% performance improvement, demonstrating our method’s superior ability to unlock ViT’s potential.

Additionally, we further evaluate the generalization of different FFD models on our 9 cross-datasets. The quantitative comparison in Table 3 shows that both our baseline BEiT v2’ and Ours outperform other FFD methods, highlighting the importance of a backbone with real face knowledge and the effectiveness of competitive forgery cue extraction. However, all listed FFD methods in Table 3 exhibit poor generalization performance on StyleGAN3-generated faces, mainly due to unseen entire face forgeries during training and the high realism of these fakes. Therefore, we employ a small number of StyleGAN3-generated forged faces (20 images) to fine-tune different methods further, enabling

TABLE 2

Quantitative generalization comparison of different FFD methods. “†” denotes the author’s trained model, “‡” indicates re-implementation using public code, and “*” signifies results from the original paper. **Bold** and underline represent the best and second-best, respectively.

Method	Venue	Cross-set AUC↑ (%)			
		CDF	DFDC	FFIW	Avg
FTCN [†] [72]	CVPR 2021	87.88	71.31	87.62	82.27
SBI [†] [55]	CVPR 2022	<u>92.87</u>	71.96	83.22	82.68
RECCE [‡] [69]	CVPR 2022	71.58	64.53	73.51	69.87
CORE [‡] [33]	CVPR 2022	80.10	70.53	78.42	76.35
UIA-ViT [†] [21]	ECCV 2022	83.75	74.34	75.82	77.97
D-adv [‡] [124]	TIP 2022	82.77	73.91	72.84	76.51
UCF [†] [17]	ICCV 2023	77.45	70.68	66.16	71.43
CADDM [†] [18]	CVPR 2023	84.39	70.46	85.72	80.19
AltFreezing [‡] [57]	CVPR 2023	89.23	72.38	75.79	79.13
LSDA [*] [20]	CVPR 2024	91.10	77.00	–	–
Choi <i>et al.</i> [*] [19]	CVPR 2024	89.00	–	–	–
BEiT v2’	-	89.18	84.02	86.48	86.56
Ours	-	90.46	<u>84.90</u>	90.97	88.78
Ours+SBI	-	95.35	85.45	91.82	90.87

TABLE 3

Quantitative generalization comparison of FFD methods across various forgery synthesis algorithms, including representative GAN-based and Diffusion Model-based methods covering four types of forgeries. Results at the bottom of this table come from FFD methods fine-tuned on 20 StyleGAN3-generated forged faces.

Forged Faces	RECCE	CORE	D-adv	CADDM	BEiT v2	BEiT v2’	Ours
1. Entire Face Synthesis							
DCGAN [116]	85.28	81.03	90.87	85.67	91.93	99.94	99.48
StyleGAN3 [13]	<u>57.25</u>	35.69	33.06	45.15	51.13	57.24	60.75
SD-1.5 [118]	82.46	66.15	66.23	49.49	80.15	<u>83.18</u>	86.84
2. Face Attribute Editing							
StarGAN2 [15]	54.71	26.62	28.20	55.92	66.03	<u>73.56</u>	79.33
AttnGAN [117]	60.35	52.13	66.42	64.99	69.87	81.15	80.11
3. Face Swapping							
E4S [14]	65.32	32.43	37.03	46.45	66.15	<u>81.30</u>	85.02
DiffFace [119]	50.07	55.08	49.66	53.42	61.28	<u>81.27</u>	82.94
4. Face Reenactment							
Wav2Lip [16]	72.71	78.43	73.00	69.48	96.92	<u>98.96</u>	99.00
Diffused Heads [120]	79.12	76.55	84.08	85.76	94.46	97.58	<u>96.44</u>
Avg AUC (%)	<u>66.82</u>	53.21	56.94	60.86	72.63	<u>81.90</u>	83.86
Forged Faces	RECCE	CORE	D-adv	CADDM	BEiT v2	BEiT v2’	Ours
StyleGAN3 [13]	<u>72.09</u>	45.21	49.05	–	57.12	71.09	82.20

verification of their rapid adaptability to unseen forgery techniques. The bottom row of Table 3 presents the adaptability performance, where RECCE [69] and BEiT v2’ show greater improvement by modeling real face features, while Ours demonstrates even more impressive performance with a 21.45% improvement, proving its superior practicality.

4.3.2 Adaptation Evaluation

Next, we evaluate the adaptation capability of various FFD methods by further fine-tuning FFD models using a few images from previously unseen common datasets, having initially trained these models on the FF++ dataset. Specifically, we conduct 10-shot and 20-shot experiments with an equal number of real and fake faces, fine-tuning the different FFD models for 2 epochs with a learning rate of $2e - 5$.

Table 4 shows the quantitative comparison results, indicating that BEiT v2’ pre-trained on real-face dataset not only adapts well to the target dataset but also maintains stable

TABLE 4

Quantitative adaptation comparison of different FFD models by further fine-tuning on a few images (10-*Shot*, 20-*Shot*) from unseen datasets. These models have been fine-tuned on the source dataset (FF++). **bold** means the best, and **bold** means the second-best. \uparrow and \downarrow indicate an increase and decrease relative to the baseline (gray), respectively. Higher values on the diagonal represent greater performance and adaptation.

Method	Training Set (10/20- <i>Shot</i>)	10- <i>Shot</i> Testing Set AUC \uparrow (%)					20- <i>Shot</i> Testing Set AUC \uparrow (%)				
		FF++	CDF	DFDC	FFIW	Avg	FF++	CDF	DFDC	FFIW	Avg
RECCE [69]	FF++	97.91	71.58	64.53	73.51	76.88	97.91	71.58	64.53	73.51	76.88
	CDF	89.25 \downarrow	67.78 \downarrow	65.45 \uparrow	66.59 \downarrow	72.27 \downarrow	93.58 \downarrow	70.45 \downarrow	61.95 \downarrow	67.50 \downarrow	73.37 \downarrow
	DFDC	92.36 \downarrow	67.00 \downarrow	67.34 \uparrow	77.36 \uparrow	76.02 \downarrow	90.31 \downarrow	68.15 \downarrow	67.00 \uparrow	77.36 \uparrow	75.71 \downarrow
	FFIW	97.66 \downarrow	67.73 \downarrow	65.22 \uparrow	73.96 \uparrow	76.14 \downarrow	94.62 \downarrow	70.31 \downarrow	66.55 \uparrow	77.49 \uparrow	77.24 \downarrow
CORE [33]	FF++	97.66	80.10	70.53	78.42	81.68	97.66	80.10	70.53	78.42	81.68
	CDF	97.77 \uparrow	81.49 \uparrow	68.91 \downarrow	77.78 \downarrow	81.49 \downarrow	97.74 \downarrow	81.77 \uparrow	68.99 \downarrow	79.85 \uparrow	82.09 \uparrow
	DFDC	97.22 \downarrow	79.06 \downarrow	74.33 \uparrow	79.85 \uparrow	82.62 \uparrow	97.14 \downarrow	78.77 \downarrow	74.93 \uparrow	79.92 \uparrow	82.69 \uparrow
	FFIW	97.51 \downarrow	81.85 \uparrow	71.21 \uparrow	78.32 \downarrow	82.22 \uparrow	97.54 \downarrow	80.82 \uparrow	71.34 \uparrow	79.14 \uparrow	82.21 \uparrow
D-adv [124]	FF++	98.31	82.77	73.91	72.84	81.96	98.31	82.77	73.91	72.84	81.96
	CDF	98.40 \uparrow	82.89 \uparrow	71.42 \downarrow	68.35 \downarrow	80.27 \downarrow	98.41 \uparrow	85.05 \uparrow	71.21 \downarrow	67.91 \downarrow	80.65 \downarrow
	DFDC	98.47 \uparrow	80.80 \downarrow	75.05 \uparrow	69.76 \downarrow	81.02 \downarrow	98.34 \uparrow	81.29 \downarrow	75.27 \downarrow	68.60 \downarrow	80.88 \downarrow
	FFIW	98.47 \uparrow	82.90 \uparrow	73.45 \downarrow	68.25 \downarrow	80.77 \downarrow	98.35 \uparrow	82.04 \downarrow	73.80 \downarrow	69.46 \downarrow	80.91 \downarrow
BEiT v2	FF++	99.16	89.48	81.00	77.61	86.81	99.16	89.48	81.00	77.61	86.81
	CDF	99.09 \downarrow	89.26 \downarrow	79.88 \downarrow	73.21 \downarrow	85.36 \downarrow	98.88 \downarrow	91.94 \uparrow	80.81 \downarrow	76.52 \downarrow	87.04 \uparrow
	DFDC	99.15 \downarrow	90.21 \uparrow	82.27 \uparrow	79.06 \uparrow	87.67 \uparrow	99.15 \downarrow	90.50 \uparrow	82.91 \uparrow	79.31 \uparrow	87.97 \uparrow
	FFIW	99.10 \downarrow	90.73 \uparrow	82.27 \uparrow	85.51 \uparrow	89.40 \uparrow	98.95 \downarrow	91.34 \uparrow	82.17 \uparrow	90.67 \uparrow	90.78 \uparrow
BEiT v2'	FF++	99.14	89.13	84.02	86.48	89.71	99.14	89.13	84.02	86.48	89.71
	CDF	99.07 \downarrow	90.83 \uparrow	84.69 \uparrow	85.97 \downarrow	90.14 \uparrow	98.70 \downarrow	92.25 \uparrow	85.63 \uparrow	89.98 \uparrow	91.64 \uparrow
	DFDC	98.79 \downarrow	91.17 \uparrow	86.63 \uparrow	91.23 \uparrow	91.96 \uparrow	98.58 \downarrow	90.11 \uparrow	87.44 \uparrow	89.94 \uparrow	91.52 \uparrow
	FFIW	98.98 \downarrow	89.21 \downarrow	86.31 \uparrow	91.83 \uparrow	91.58 \uparrow	98.97 \downarrow	90.60 \uparrow	87.27 \uparrow	95.14 \uparrow	93.00 \uparrow
Ours	FF++	99.36	90.46	84.90	90.97	91.42	99.36	90.46	84.90	90.97	91.42
	CDF	99.25 \downarrow	91.33 \uparrow	86.17 \uparrow	91.74 \uparrow	92.12 \uparrow	99.10 \downarrow	91.31 \uparrow	85.48 \uparrow	91.82 \uparrow	91.93 \uparrow
	DFDC	99.10 \downarrow	91.16 \uparrow	87.72 \uparrow	93.23 \uparrow	92.80 \uparrow	98.92 \downarrow	91.08 \uparrow	88.07 \uparrow	91.80 \uparrow	92.47 \uparrow
	FFIW	99.22 \downarrow	90.14 \uparrow	85.78 \uparrow	93.65 \uparrow	92.20 \uparrow	99.09 \downarrow	91.11 \uparrow	86.78 \uparrow	96.65 \uparrow	93.41 \uparrow

performance in the source dataset (FF++), whereas previous methods suffer varying degrees of performance degradation. Meanwhile, our model performs best in target and unseen cross-datasets, demonstrating that our competitive backbone fine-tuning framework has superior practicability and robustness. Notably, Ours improves by 2.82% (AUC \uparrow : 84.90% vs. 87.72%) on DFDC with 5,000 test images under the 10-shot condition, and by 3.17% (84.90% vs. 88.07%) on DFDC and 5.68% (90.97% vs. 96.65%) on FFIW under the 20-shot condition, highlighting the effectiveness of our expert knowledge-equipped backbone in identifying forgery cues and efficiently adapting to unknown forgery patterns.

4.4 Analysis of Backbone Fine-tuning Framework

We then analyze the efficacy of our competitive backbone fine-tuning framework through the following aspects: (1) decorrelation loss \mathcal{L}_{dec} , (2) Uncertainty-based Fusion Module (UFM), (3) Evidence Deep Learning and Evidential Uncertainty Calibration losses \mathcal{L}_{EDU} , (4) our framework with different backbones, (5) attention map and feature visualizations, and (6) additional on real-face datasets.

Table 5 shows the quantitative comparison results of core components in our framework, as can be seen: (1) without \mathcal{L}_{dec} , the dual-branch backbone tends to learn similar forgery cues, resulting in only a slight improvement over BEiT v2' under the fusion module with sum operation; (2) incorporating \mathcal{L}_{dec} can better promote the generalization of the main branch, with the average AUC improving from 87.04% to 88.14%; (3) our framework with UFM provides dynamic weights for feature fusion based on the prediction uncertainties of the main and auxiliary branches, enhancing

TABLE 5

Quantitative comparison of our framework with different components. Without UFM, we sum features from dual branches. When \mathcal{L}_{EDU} is not used, \mathcal{L}_{ce} is used instead. The results of our auxiliary branch (Ours_A) and both branches (Ours_M+A) are presented as reference.

Method	\mathcal{L}_{dec}	UFM	\mathcal{L}_{EDU}	Cross-set AUC \uparrow (%)			Avg \uparrow (%)	
				CDF	DFDC	FFIW	AUC	ACC
BEiT v2'			\checkmark	89.18	84.02	86.48	86.56	79.37
				89.34	84.19	88.76	87.43	80.96
Ours	\checkmark			89.77	83.67	87.69	87.04	79.26
	\checkmark	\checkmark		90.31	84.89	89.21	88.14	79.42
	\checkmark	\checkmark	\checkmark	91.16	84.54	90.22	88.64	80.84
Ours_A	\checkmark	\checkmark	\checkmark	90.46	84.90	90.97	88.78	82.29
Ours_M+A	\checkmark	\checkmark	\checkmark	79.83	68.29	68.97	72.36	67.96
	\checkmark	\checkmark	\checkmark	90.45	83.10	89.72	87.76	82.04

their competition and improving backbone performance; (4) \mathcal{L}_{EDU} further enhances the model's FFD capability by constraining prediction uncertainty and class probability.

Additionally, although the Avg AUC \uparrow performance improvement of our framework with UFM and \mathcal{L}_{EDU} is not very large compared to not using them (88.78% vs. 88.14%), we are the first to introduce model uncertainty estimation in FFD solutions and propose a novel uncertainty-based threshold optimization mechanism for FFD models during the *inference* stage, thereby significantly enhancing the accuracy of FFD models in discriminant results (Avg ACC \uparrow : 79.42% vs. 82.29%). Please refer to Section 4.5 for more analysis. Besides, we also present a comparison of the auxiliary branch (Ours_A) and both branches (Ours_M+A) in our framework. Both Ours_A and Ours_M+A perform lower than the main branch (Ours), demonstrating the effectiveness of our competitive learning mechanism, which

TABLE 6

Quantitative comparison of our framework with different backbones.

Method	In-set	Cross-set AUC↑ (%)				
	FF++	CDF	DFDC	FFIW	Avg	
ViT (SL on 1k)	97.09	83.39	76.77	71.17	77.11	
Ours <i>w/</i> ViT (SL on 1k)	97.10	83.41	78.33	75.09	78.94	
MAE' (1k&Face)	98.37	85.85	78.04	78.07	80.65	
Ours <i>w/</i> MAE' (1k&Face)	97.97	85.91	79.05	81.16	82.04	
MoCo v3' (1k&Face)	98.65	84.98	79.13	85.72	83.28	
Ours <i>w/</i> MoCo v3' (1k&Face)	98.48	88.02	79.17	89.19	85.46	
BEiT v2' (1k&Face)	99.14	89.18	84.02	86.48	86.56	
Ours <i>w/</i> BEiT v2' (1k&Face)	99.36	90.46	84.90	90.97	88.78	

TABLE 7

Quantitative comparison of pre-training on different scales of real faces.

Method	Real Faces	In-set	Cross-set AUC ↑ (%)			
		FF++	CDF	DFDC	FFIW	Avg
BEiT v2'	55w	99.14	89.18	84.02	86.48	86.56
	750w	99.21	90.76	86.77	88.82	88.78
Ours	55w	99.36	90.46	84.90	90.97	88.78
	750w	99.13	90.99	86.79	90.72	89.50

significantly fosters the main backbone’s generalization.

We further validate the flexibility of our competitive backbone fine-tuning framework by using backbones pre-trained with different learning approaches and datasets, including ViT with SL on ImageNet-1k (SL on 1K), MAE, MoCo v3, and BEiT v2. The quantitative comparison in Table 6 shows that our framework with different backbones achieves around 2% performance improvement, further demonstrating the robustness and potential of our competitive learning mechanism with the decorrelation constraint and uncertainty-based fusion module.

Moreover, to explain the performance improvement of our method, we visualize attention maps to show the model’s focus areas on the face and perform cluster analysis of the output in the feature space. For attention map visualization, we utilize Attention Rollout [32], which averages the attention weights across all heads and recursively multiplies them by the weight matrices of all layers in the backbone. Figure 6 illustrates that BEiT v2 better focuses on local facial components compared to the supervised learning approach. After real-face pre-training, BEiT v2’ effectively targets local forgery areas, while our model is even more precise, leading to more accurate and reliable detection results. For cluster analysis, we use t-SNE [125] to present the feature vectors of the last layer of the backbone. The isolated features of real and four forgery algorithms (Deepfakes, Face2Face, FaceSwap, NeuralTextures) in BEiT v2, as shown in Figure 7, indicate that BEiT v2 mainly learns method-specific types rather than general forgeries, making it difficult to generalize to a broader range of forgeries. In contrast, BEiT v2’ primarily distinguishes real and fake faces thanks to its robust facial representation capabilities from real face pre-training. Meanwhile, our model better clusters real faces and separates them from fake faces, indicating that it more effectively extracts implicit forgery cues for generalization.

Additionally, given the importance of specific knowledge from real faces for backbones in representing facial features, we introduce a larger-scale real-face dataset to validate its FFD performance. We build a 7,500,000 real-

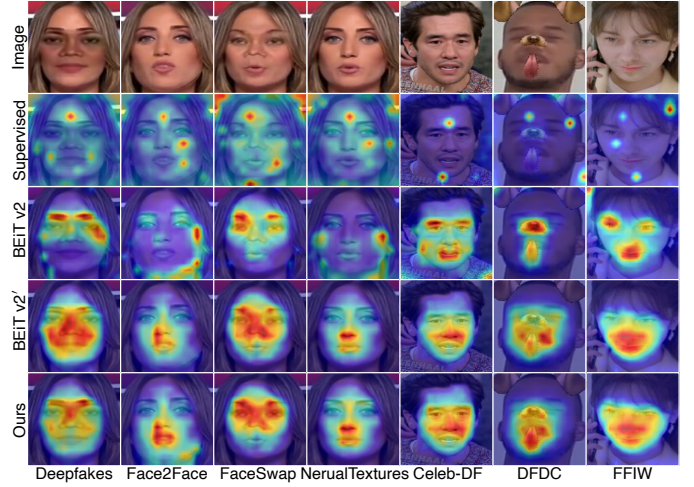


Fig. 6. Visualization of attention maps for FFD methods on different forgery techniques. Highlighted areas indicate higher model attention.

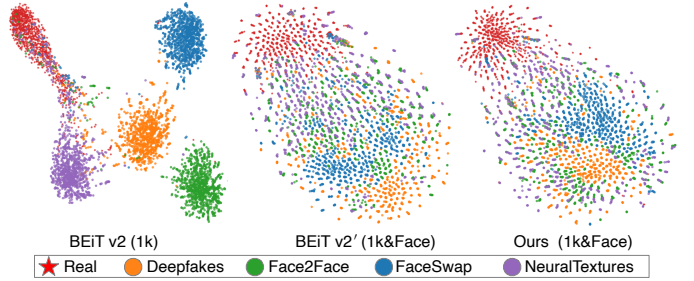


Fig. 7. The t-SNE visualization of last-layer feature vectors from different backbones. Better generalization of the FFD model is indicated by more clustered real points and more dispersed other points.

face dataset based on MSCelebV1 [126], MegaFace [127], and LAION-Face [128] to further pre-train BEiT v2. The quantitative results in Table 7 show that adding more real faces can further improve FFD performance, with our framework demonstrating the best results, despite the difficulty of further improvement at higher performance levels.

4.5 Analysis of Threshold Optimization Mechanism

We conduct experiments to validate the critical role of the classification threshold τ in FFD final discriminant results. Our study includes the empirical value of 0.5, using the optimal thresholds τ_{ot} from one cross-dataset to another, and our uncertainty-based threshold optimization mechanism (UTOM). Meanwhile, we compare \mathcal{L}_{EDU} and \mathcal{L}_{ce} to verify their impact on uncertainty and predicted probability.

Table 8 and Figure 8 show the quantitative and visual statistical comparison results, respectively. As can be seen, τ_{ot} from one cross-dataset achieves better ACC on other cross-datasets compared to $\tau=0.5$, and our UTOM performs the best. \mathcal{L}_{EDU} also achieves better ACC compared to \mathcal{L}_{ce} , indicating that constraining uncertainty and predicted probability improves the model’s confidence in its predictions. Remarkably, our UTOM with \mathcal{L}_{EDU} achieves a significant ACC improvement over the default optimal threshold (OT with \mathcal{L}_{ce}) in both BEiT v2’ and our model, with an average ACC increase of more than 2%, fully demonstrates the reli-

TABLE 8

Quantitative ACC↑ (%) comparison of different classification thresholds in FFD models with \mathcal{L}_{EDU} or \mathcal{L}_{ce} . 0.5 is the empirical threshold. OT and OT w/ U denote the default and our UTOM-adjusted optimal thresholds, respectively. **Bold** and underline indicate the best and second-best results.

Method	Loss	Threshold	CDF to CDF&DFDC&FFIW				DFDC to CDF&DFDC&FFIW				FFIW to CDF&DFDC&FFIW				Avg
			CDF	DFDC	FFIW	Avg	CDF	DFDC	FFIW	Avg	CDF	DFDC	FFIW	Avg	
BEiT v2'	\mathcal{L}_{ce}	0.5	77.61	72.00	76.00	75.20	77.61	72.00	76.00	75.20	77.61	72.00	76.00	75.20	75.20
		OT	83.40	75.40	78.00	78.93	80.69	76.02	76.60	77.77	81.47	75.00	80.20	78.89	78.53
		OT w/ U	83.01	75.70	79.60	79.44	81.85	75.80	80.20	79.28	82.05	75.76	80.40	79.40	79.37
	\mathcal{L}_{EDU}	0.5	80.12	73.42	78.40	77.31	80.12	73.42	78.40	77.31	80.12	73.42	78.40	77.31	77.31
		OT	81.85	76.12	77.60	78.52	81.27	76.32	78.60	78.73	80.31	75.70	82.00	79.34	78.86
		OT w/ U	82.05	<u>76.94</u>	<u>82.00</u>	80.33	80.89	<u>77.56</u>	84.00	81.22	80.89	<u>77.52</u>	85.60	<u>81.34</u>	<u>80.96</u>
Ours	\mathcal{L}_{ce}	0.5	83.40	75.70	81.40	80.17	83.40	75.70	81.40	80.17	83.40	<u>75.70</u>	81.40	80.17	80.17
		OT	83.98	75.84	81.20	80.34	83.01	76.68	81.20	80.30	82.24	76.16	82.60	80.33	80.32
		OT w/ U	84.36	76.54	80.00	80.30	83.59	77.50	82.60	81.23	82.82	77.38	82.80	81.00	80.84
	\mathcal{L}_{EDU}	0.5	83.20	76.00	81.20	80.13	83.20	76.00	81.20	80.13	<u>83.20</u>	76.00	81.20	80.13	80.13
		OT	83.78	75.94	81.40	80.37	81.66	77.06	82.20	80.31	82.63	76.76	84.20	81.20	80.63
		OT w/ U	85.33	77.54	83.80	82.22	84.75	78.66	84.00	82.47	83.40	78.30	<u>84.80</u>	82.17	82.29

TABLE 9

Quantitative comparison of different PAD methods from three source datasets to one target dataset.

Method	Venue	O&C&I to M		O&M&I to C		O&C&M to I		I&C&M to O		Avg	
		HTER↓ (%)	AUC↑ (%)								
SSDG [41]	CVPR 2020	7.38	97.17	10.44	95.94	11.71	96.59	15.61	91.54	11.29	95.31
PatchNet [45]	CVPR 2022	7.10	98.46	11.33	94.58	13.4	95.67	11.82	95.07	10.91	95.95
SSAN [43]	CVPR 2022	6.67	98.75	10.00	96.67	8.88	96.79	13.72	93.63	9.82	96.46
DSCI [46]	TIFS 2023	<u>5.48</u>	97.39	<u>8.00</u>	<u>97.50</u>	5.71	98.44	12.59	94.57	7.95	96.98
UDG [47]	ICCV 2023	5.95	98.47	9.82	96.76	5.86	98.62	10.97	95.36	8.15	<u>97.30</u>
GAC-FAS [129]	CVPR 2024	5.00	97.56	8.20	95.16	<u>4.29</u>	<u>98.87</u>	<u>8.60</u>	<u>97.16</u>	<u>6.52</u>	<u>97.19</u>
Ours	—	5.95	<u>98.52</u>	3.44	99.63	2.93	99.58	5.68	98.17	4.50	98.98

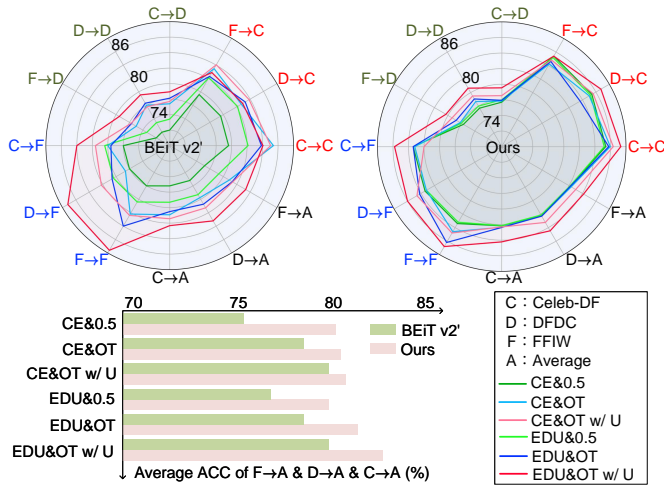


Fig. 8. Visual statistical comparison of different classification thresholds under FFD models with \mathcal{L}_{EDU} (EDU) or \mathcal{L}_{ce} (CE). 0.5 is the empirical threshold. OT and OT w/ U denote the default and our UTOM-adjusted optimal thresholds, respectively. X→Y represents applying the optimal threshold of X to the Y dataset.

ability of our UTOM in FFD applications, as well as the importance of our fine-tuning framework with the uncertainty-based fusion module (UFM) and \mathcal{L}_{EDU} . Moreover, the comparison results on FFIW using τ_{ot} from other cross-datasets, such as C→F and D→F in Figure 8(left), show that FFIW’s ACC is particularly sensitive to the τ_{ot} , indicating significant differences in forgery patterns between FFIW and other cross-datasets. Fortunately, as shown in Figure 8(right), our model maintains stable ACC on FFIW, further confirming its strong generalization performance.

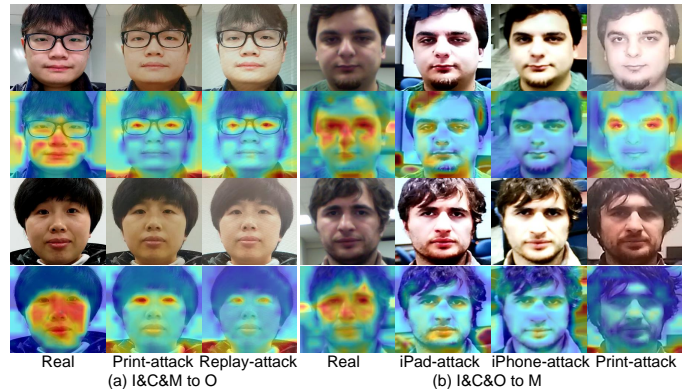


Fig. 9. Visualization of attention maps from our PAD model on different target datasets. The model focuses on most facial regions in real faces, while highlighting inconsistent areas in fake faces.

5 BEYOND THE FACE FORGERY DETECTION

We extend our exploration of the backbone’s *pre-training* and *fine-tuning* stages to the face-related task of presentation attack detection (PAD), which also aims to distinguish the authenticity of input faces. We conduct experiments on four commonly used public datasets: OULU-NPU [130] (O), CASIA-FASD [131] (C), Idiap Replay-Attack [132] (I), and MSU-MFSD [133] (M). We follow the evaluation protocol and data preprocessing process of SSDG [41]. One dataset is used as the target domain for evaluation, while the other three serve as source domains for fine-tuning, *i.e.*, O&C&I to M, O&M&I to C, O&C&M to I, and I&C&M to O.

We evaluate our PAD model against the state-of-the-art methods: SSDG [41], PatchNet [45], SSAN [43], DSCI [46],

UDG [47], and GAC-FAS [129]. Table 9 presents the comparison results, showing that our model performs excellently on HTER and AUC metrics. Especially, our model outperforms GAC-FAS [129] on the challenging OULU-NPU dataset (I&C&M to O) with an improvement of 1.01% in AUC \uparrow (98.17% vs. 97.16%) and a reduction of 2.92% in HTER \downarrow (5.68% vs. 8.60%). Additionally, the AUC \uparrow of our model on the CASIA-FASD (O&M&I to C) and Idiap Replay-Attack (O&C&M to I) datasets exceeds 99%. Moreover, we also visualize our model’s attention map on PAD in Figure 9, indicating that our model can represent real faces by focusing on the facial region, while fake face images pay attention to inconsistent clues such as light, texture, and background.

6 CONCLUSION

In this paper, we present insightful guidance and practical solutions for FFD research through a complete revisiting of FFD workflow and an empirical study of backbones with various configurations. We revitalize the traditional FFD pipeline by introducing SSL on real faces, a competitive backbone framework, and a threshold optimization mechanism in the *pre-training*, *fine-tuning*, and *inference* stages, respectively, thereby developing an elaborate backbone tailored for FFD generalization. Moreover, we leverage uncertainty estimation and evidential deep learning to design an uncertainty-based fusion module for fine-tuning and an adjusted prediction probability strategy to handle magnified confidence issues, enhancing the backbone’s generalization and reliability. We conduct comprehensive experiments to demonstrate the practicality of our solution and its method. Additionally, we extend our method to PAD task, further illustrating the superiority of our method. We hope our work opens up new avenues for FFD and PAD tasks.

ACKNOWLEDGMENTS

This work was supported by the National Natural Science Foundation of China (No. 62276249 and No. 62171421), the Strategic Priority Research Program of the Chinese Academy of Sciences (No. XDB0680000), the Fundamental Research Funds for the Central Universities (No. 202461014), the TaiShan Scholars Youth Expert Program of Shandong Province (No. tsqn202306096), the Beijing Nova Program (No. 20230484368), and the Youth Innovation Promotion Association CAS.

REFERENCES

- [1] M. Wang and W. Deng, “Deep face recognition: A survey,” *Neurocomputing*, vol. 429, pp. 215–244, 2021.
- [2] W. Zhang, S. Shan, W. Gao, X. Chen, and H. Zhang, “Local gabor binary pattern histogram sequence (lgbphs): A novel non-statistical model for face representation and recognition,” in *IEEE/CVF Int. Conf. Comput. Vis.*, 2005, pp. 786–791.
- [3] M. Toshpulatov, W. Lee, and S. Lee, “Talking human face generation: A survey,” *Expert Systems with Applications*, vol. 219, p. 119678, 2023.
- [4] A. Melnik, M. Miasayedzenkau, D. Makaravets, D. Pirshutuk, E. Akbulut, D. Holzmann, T. Renusch, G. Reichert, and H. Ritter, “Face generation and editing with stylegan: A survey,” *IEEE Trans. Pattern Anal. Mach. Intell.*, 2024.
- [5] X. Zheng, Y. Guo, H. Huang, Y. Li, and R. He, “A survey of deep facial attribute analysis,” *Int. J. Comput. Vis.*, vol. 128, pp. 2002–2034, 2020.
- [6] A. R. Rivera, J. R. Castillo, and O. O. Chae, “Local directional number pattern for face analysis: Face and expression recognition,” *IEEE Trans. Image Process.*, vol. 22, no. 5, pp. 1740–1752, 2012.
- [7] Y. Choi, Y. Uh, J. Yoo, and J.-W. Ha, “Stargan v2: Diverse image synthesis for multiple domains,” in *IEEE/CVF Conf. Comput. Vis. Pattern Recog.*, 2020, pp. 8188–8197.
- [8] E. Richardson, Y. Alaluf, O. Patashnik, Y. Nitzan, Y. Azar, S. Shapiro, and D. Cohen-Or, “Encoding in style: a stylegan encoder for image-to-image translation,” in *IEEE/CVF Conf. Comput. Vis. Pattern Recog.*, 2021, pp. 2287–2296.
- [9] L. Yang, Z. Zhang, Y. Song, S. Hong, R. Xu, Y. Zhao, W. Zhang, B. Cui, and M.-H. Yang, “Diffusion models: A comprehensive survey of methods and applications,” *ACM Comput. Surv.*, vol. 56, no. 4, pp. 1–39, 2023.
- [10] Y. Mirsky and W. Lee, “The creation and detection of deepfakes: A survey,” *ACM Comput. Surv.*, vol. 54, no. 1, pp. 1–41, 2021.
- [11] T. T. Nguyen, Q. V. H. Nguyen, D. T. Nguyen, D. T. Nguyen, T. Huynh-The, S. Nahavandi, T. T. Nguyen, Q.-V. Pham, and C. M. Nguyen, “Deep learning for deepfakes creation and detection: A survey,” *Computer Vision and Image Understanding*, vol. 223, p. 103525, 2022.
- [12] R. Tolosana, R. Vera-Rodriguez, J. Fierrez, A. Morales, and J. Ortega-Garcia, “Deepfakes and beyond: A survey of face manipulation and fake detection,” *Information Fusion*, vol. 64, pp. 131–148, 2020.
- [13] T. Karras, M. Aittala, S. Laine, E. Härkönen, J. Hellsten, J. Lehtinen, and T. Aila, “Alias-free generative adversarial networks,” in *Adv. Neural Inf. Process. Syst.*, 2021.
- [14] Z. Liu, M. Li, Y. Zhang, C. Wang, Q. Zhang, J. Wang, and Y. Nie, “Fine-grained face swapping via regional gan inversion,” in *IEEE/CVF Conf. Comput. Vis. Pattern Recog.*, 2023, pp. 8578–8587.
- [15] Y. Choi, Y. Uh, J. Yoo, and J.-W. Ha, “Stargan v2: Diverse image synthesis for multiple domains,” in *IEEE/CVF Conf. Comput. Vis. Pattern Recog.*, 2020.
- [16] K. Prajwal, R. Mukhopadhyay, V. P. Namboodiri, and C. Jawahar, “A lip sync expert is all you need for speech to lip generation in the wild,” in *ACM MM*, 2020, pp. 484–492.
- [17] Z. Yan, Y. Zhang, Y. Fan, and B. Wu, “Ucf: Uncovering common features for generalizable deepfake detection,” in *IEEE/CVF Conf. Comput. Vis. Pattern Recog.*, 2023, pp. 22 412–22 423.
- [18] S. Dong, J. Wang, R. Ji, J. Liang, H. Fan, and Z. Ge, “Implicit identity leakage: The stumbling block to improving deepfake detection generalization,” in *IEEE/CVF Conf. Comput. Vis. Pattern Recog.*, 2023, pp. 3994–4004.

- [19] J. Choi, T. Kim, Y. Jeong, S. Baek, and J. Choi, "Exploiting style latent flows for generalizing deepfake video detection," in *IEEE/CVF Conf. Comput. Vis. Pattern Recog.*, 2024, pp. 1133–1143.
- [20] Z. Yan, Y. Luo, S. Lyu, Q. Liu, and B. Wu, "Transcending forgery specificity with latent space augmentation for generalizable deepfake detection," in *IEEE/CVF Conf. Comput. Vis. Pattern Recog.*, June 2024, pp. 8984–8994.
- [21] W. Zhuang, Q. Chu, Z. Tan, Q. Liu, H. Yuan, C. Miao, Z. Luo, and N. Yu, "Uia-vit: Unsupervised inconsistency-aware method based on vision transformer for face forgery detection," in *Eur. Conf. Comput. Vis.* Springer, 2022, pp. 391–407.
- [22] L. Jing and Y. Tian, "Self-supervised visual feature learning with deep neural networks: A survey," *IEEE Trans. Pattern Anal. Mach. Intell.*, vol. 43, no. 11, pp. 4037–4058, 2020.
- [23] Z. Xie, Z. Zhang, Y. Cao, Y. Lin, J. Bao, Z. Yao, Q. Dai, and H. Hu, "Simmim: A simple framework for masked image modeling," in *IEEE/CVF Conf. Comput. Vis. Pattern Recog.*, 2022, pp. 9653–9663.
- [24] K. He, X. Chen, S. Xie, Y. Li, P. Dollár, and R. Girshick, "Masked autoencoders are scalable vision learners," in *IEEE/CVF Conf. Comput. Vis. Pattern Recog.*, 2022, pp. 16 000–16 009.
- [25] Z. Peng, L. Dong, H. Bao, Q. Ye, and F. Wei, "BEiT v2: Masked image modeling with vector-quantized visual tokenizers," *arXiv preprint arXiv:2208.06366*, 2022.
- [26] W. Wang, H. Bao, L. Dong, J. Bjorck, Z. Peng, Q. Liu, K. Aggarwal, O. K. Mohammed, S. Singhal, S. Som *et al.*, "Image as a foreign language: Beit pretraining for vision and vision-language tasks," in *IEEE/CVF Conf. Comput. Vis. Pattern Recog.*, 2023, pp. 19 175–19 186.
- [27] A. Radford, J. W. Kim, C. Hallacy, A. Ramesh, G. Goh, S. Agarwal, G. Sastry, A. Askell, P. Mishkin, J. Clark *et al.*, "Learning transferable visual models from natural language supervision," in *Int. Conf. Mach. Learn.* PMLR, 2021, pp. 8748–8763.
- [28] A. Radford, K. Narasimhan, T. Salimans, I. Sutskever *et al.*, "Improving language understanding by generative pre-training," *OpenAI*, 2018.
- [29] K. He, X. Zhang, S. Ren, and J. Sun, "Deep residual learning for image recognition," in *IEEE Conf. Comput. Vis. Pattern Recog.*, 2016, pp. 770–778.
- [30] F. Chollet, "Xception: Deep learning with depthwise separable convolutions," in *IEEE Conf. Comput. Vis. Pattern Recog.*, 2017, pp. 1251–1258.
- [31] M. Tan and Q. Le, "Efficientnet: Rethinking model scaling for convolutional neural networks," in *Int. Conf. Mach. Learn.* PMLR, 2019, pp. 6105–6114.
- [32] A. Dosovitskiy, L. Beyer, A. Kolesnikov, D. Weissenborn, X. Zhai, T. Unterthiner, M. Dehghani, M. Minderer, G. Heigold, S. Gelly, J. Uszkoreit, and N. Houlsby, "An image is worth 16x16 words: Transformers for image recognition at scale," *ICLR*, 2021.
- [33] Y. Ni, D. Meng, C. Yu, C. Quan, D. Ren, and Y. Zhao, "Core: Consistent representation learning for face forgery detection," in *IEEE/CVF Conf. Comput. Vis. Pattern Recog.*, 2022, pp. 12–21.
- [34] L. Hu, M. Kan, S. Shan, X. Song, and X. Chen, "Ldf-net: Learning a displacement field network for face recognition across pose," in *2017 12th IEEE International Conference on Automatic Face & Gesture Recognition (FG 2017)*. IEEE, 2017, pp. 9–16.
- [35] M. He, J. Zhang, S. Shan, M. Kan, and X. Chen, "Deformable face net for pose invariant face recognition," *PR*, vol. 100, p. 107113, 2020.
- [36] B. Lakshminarayanan, A. Pritzel, and C. Blundell, "Simple and scalable predictive uncertainty estimation using deep ensembles," *Adv. Neural Inf. Process. Syst.*, vol. 30, 2017.
- [37] A. Kendall and Y. Gal, "What uncertainties do we need in bayesian deep learning for computer vision?" *Adv. Neural Inf. Process. Syst.*, vol. 30, 2017.
- [38] A. George, Z. Mostaani, D. Geissenbuhler, O. Nikisins, A. Anjos, and S. Marcel, "Biometric face presentation attack detection with multi-channel convolutional neural network," *IEEE Trans. Inf. Forensics Security.*, vol. 15, pp. 42–55, 2019.
- [39] R. Tolosana, M. Gomez-Barrero, C. Busch, and J. Ortega-Garcia, "Biometric presentation attack detection: Beyond the visible spectrum," *IEEE Trans. Inf. Forensics Security.*, vol. 15, pp. 1261–1275, 2019.
- [40] E. Park, X. Cui, T. H. B. Nguyen, and H. Kim, "Presentation attack detection using a tiny fully convolutional network," *IEEE Trans. Inf. Forensics Security.*, vol. 14, no. 11, pp. 3016–3025, 2019.
- [41] Y. Jia, J. Zhang, S. Shan, and X. Chen, "Single-side domain generalization for face anti-spoofing," in *IEEE/CVF Conf. Comput. Vis. Pattern Recog.*, 2020, pp. 8484–8493.
- [42] Y. Jia, J. Zhang, and S. Shan, "Dual-branch meta-learning network with distribution alignment for face anti-spoofing," *IEEE Trans. Inf. Forensics Security.*, vol. 17, pp. 138–151, 2021.
- [43] Z. Wang, Z. Wang, Z. Yu, W. Deng, J. Li, T. Gao, and Z. Wang, "Domain generalization via shuffled style assembly for face anti-spoofing," in *IEEE/CVF Conf. Comput. Vis. Pattern Recog.*, 2022, pp. 4123–4133.
- [44] Z. Chen, T. Yao, K. Sheng, S. Ding, Y. Tai, J. Li, F. Huang, and X. Jin, "Generalizable representation learning for mixture domain face anti-spoofing," in *AAAI*, vol. 35, no. 2, 2021, pp. 1132–1139.
- [45] C.-Y. Wang, Y.-D. Lu, S.-T. Yang, and S.-H. Lai, "Patchnet: A simple face anti-spoofing framework via fine-grained patch recognition," in *IEEE/CVF Conf. Comput. Vis. Pattern Recog.*, 2022, pp. 20 281–20 290.
- [46] X. Long, J. Zhang, S. Wu, X. Jin, and S. Shan, "Dual sampling based causal intervention for face anti-spoofing with identity debiasing," *IEEE Trans. Inf. Forensics Security.*, 2023.
- [47] Y. Liu, Y. Chen, M. Gou, C.-T. Huang, Y. Wang, W. Dai, and H. Xiong, "Towards unsupervised domain generalization for face anti-spoofing," in *IEEE/CVF Int. Conf. Comput. Vis.*, 2023, pp. 20 654–20 664.
- [48] W. Kim, S. Suh, and J.-J. Han, "Face liveness detection from a single image via diffusion speed model," *IEEE Trans. Image Process.*, vol. 24, no. 8, pp. 2456–2465, 2015.
- [49] P. P. Chan, W. Liu, D. Chen, D. S. Yeung, F. Zhang, X. Wang, and C.-C. Hsu, "Face liveness detection us-

- ing a flash against 2d spoofing attack," *IEEE Trans. Inf. Forensics Security.*, vol. 13, no. 2, pp. 521–534, 2017.
- [50] J. Yang, Z. Lei, S. Liao, and S. Z. Li, "Face liveness detection with component dependent descriptor," in *2013 International Conference on Biometrics (ICB)*. IEEE, 2013, pp. 1–6.
- [51] Z. Yu, Y. Qin, X. Li, C. Zhao, Z. Lei, and G. Zhao, "Deep learning for face anti-spoofing: A survey," *IEEE Trans. Pattern Anal. Mach. Intell.*, vol. 45, no. 5, pp. 5609–5631, 2022.
- [52] A. Rossler, D. Cozzolino, L. Verdoliva, C. Riess, J. Thies, and M. Nießner, "Faceforensics++: Learning to detect manipulated facial images," in *IEEE/CVF Int. Conf. Comput. Vis.*, 2019, pp. 1–11.
- [53] Y. Li, X. Yang, P. Sun, H. Qi, and S. Lyu, "Celeb-df: A large-scale challenging dataset for deepfake forensics," in *IEEE/CVF Conf. Comput. Vis. Pattern Recog.*, 2020, pp. 3207–3216.
- [54] B. Dolhansky, J. Bitton, B. Pflaum, J. Lu, R. Howes, M. Wang, and C. C. Ferrer, "The deepfake detection challenge (dfdc) dataset," *arXiv preprint arXiv:2006.07397*, 2020.
- [55] K. Shiohara and T. Yamasaki, "Detecting deepfakes with self-blended images," in *IEEE/CVF Conf. Comput. Vis. Pattern Recog.*, 2022, pp. 18720–18729.
- [56] L. Li, J. Bao, T. Zhang, H. Yang, D. Chen, F. Wen, and B. Guo, "Face x-ray for more general face forgery detection," in *IEEE/CVF Conf. Comput. Vis. Pattern Recog.*, 2020, pp. 5001–5010.
- [57] Z. Wang, J. Bao, W. Zhou, W. Wang, and H. Li, "Altfreezing for more general video face forgery detection," in *IEEE/CVF Conf. Comput. Vis. Pattern Recog.*, 2023, pp. 4129–4138.
- [58] H. Dang, F. Liu, J. Stehouwer, X. Liu, and A. K. Jain, "On the detection of digital face manipulation," in *IEEE/CVF Conf. Comput. Vis. Pattern Recog.*, 2020, pp. 5781–5790.
- [59] C. Miao, Q. Chu, W. Li, S. Li, Z. Tan, W. Zhuang, and N. Yu, "Learning forgery region-aware and id-independent features for face manipulation detection," *IEEE Transactions on Biometrics, Behavior, and Identity Science*, vol. 4, no. 1, pp. 71–84, 2021.
- [60] C. Wang and W. Deng, "Representative forgery mining for fake face detection," in *IEEE/CVF Conf. Comput. Vis. Pattern Recog.*, 2021, pp. 14923–14932.
- [61] H. Zhao, W. Zhou, D. Chen, T. Wei, W. Zhang, and N. Yu, "Multi-attentional deepfake detection," in *IEEE/CVF Conf. Comput. Vis. Pattern Recog.*, 2021, pp. 2185–2194.
- [62] J. Fei, Y. Dai, P. Yu, T. Shen, Z. Xia, and J. Weng, "Learning second order local anomaly for general face forgery detection," in *IEEE/CVF Conf. Comput. Vis. Pattern Recog.*, 2022, pp. 20270–20280.
- [63] K. Sun, H. Liu, T. Yao, X. Sun, S. Chen, S. Ding, and R. Ji, "An information theoretic approach for attention-driven face forgery detection," in *Eur. Conf. Comput. Vis.* Springer, 2022, pp. 111–127.
- [64] D. Cozzolino, J. Thies, A. Rössler, C. Riess, M. Nießner, and L. Verdoliva, "Forensictransfer: Weakly-supervised domain adaptation for forgery detection," *arXiv preprint arXiv:1812.02510*, 2018.
- [65] J. Hu, S. Wang, and X. Li, "Improving the generalization ability of deepfake detection via disentangled representation learning," in *ICIP*, 2021, pp. 3577–3581.
- [66] J. Liang, H. Shi, and W. Deng, "Exploring disentangled content information for face forgery detection," in *Eur. Conf. Comput. Vis.* Springer, 2022, pp. 128–145.
- [67] B. Yan, C.-T. Li, and X. Lu, "Deepfake detection via joint unsupervised reconstruction and supervised classification," *arXiv preprint arXiv:2211.13424*, 2022.
- [68] X. Li, R. Ni, P. Yang, Z. Fu, and Y. Zhao, "Artifacts-disentangled adversarial learning for deepfake detection," *IEEE Trans. Circuits Syst. Video Technol.*, vol. 33, no. 4, pp. 1658–1670, 2022.
- [69] J. Cao, C. Ma, T. Yao, S. Chen, S. Ding, and X. Yang, "End-to-end reconstruction-classification learning for face forgery detection," in *IEEE/CVF Conf. Comput. Vis. Pattern Recog.*, 2022, pp. 4113–4122.
- [70] S. Yang, S. Hu, B. Zhu, Y. Fu, S. Lyu, X. Wu, and X. Wang, "Improving cross-dataset deepfake detection with deep information decomposition," *arXiv preprint arXiv:2310.00359*, 2023.
- [71] Y. Guo, C. Zhen, and P. Yan, "Controllable guide-space for generalizable face forgery detection," in *IEEE/CVF Int. Conf. Comput. Vis.*, 2023, pp. 20818–20827.
- [72] Y. Zheng, J. Bao, D. Chen, M. Zeng, and F. Wen, "Exploring temporal coherence for more general video face forgery detection," in *IEEE/CVF Int. Conf. Comput. Vis.*, 2021, pp. 15044–15054.
- [73] W. Haiwei, Z. Jiantao, Z. Shile, and T. Jinyu, "Exploring spatial-temporal features for deepfake detection and localization," *arXiv preprint arXiv:2210.15872*, 2022.
- [74] J. Wang, Z. Wu, W. Ouyang, X. Han, J. Chen, Y.-G. Jiang, and S.-N. Li, "M2tr: Multi-modal multi-scale transformers for deepfake detection," in *ICMR*, 2022, pp. 615–623.
- [75] C. Miao, Z. Tan, Q. Chu, H. Liu, H. Hu, and N. Yu, "F 2 trans: High-frequency fine-grained transformer for face forgery detection," *IEEE Trans. Inf. Forensics Security.*, vol. 18, pp. 1039–1051, 2023.
- [76] Y. Wang, K. Yu, C. Chen, X. Hu, and S. Peng, "Dynamic graph learning with content-guided spatial-frequency relation reasoning for deepfake detection," in *IEEE/CVF Conf. Comput. Vis. Pattern Recog.*, 2023, pp. 7278–7287.
- [77] L. Chen, Y. Zhang, Y. Song, L. Liu, and J. Wang, "Self-supervised learning of adversarial example: Towards good generalizations for deepfake detection," in *IEEE/CVF Int. Conf. Comput. Vis.*, 2022, pp. 18710–18719.
- [78] X. Wang, H. Chen, S. Tang, Z. Wu, and W. Zhu, "Disentangled representation learning," *arXiv preprint arXiv:2211.11695*, 2022.
- [79] S. Dong, J. Wang, J. Liang, H. Fan, and R. Ji, "Explaining deepfake detection by analysing image matching," in *Eur. Conf. Comput. Vis.* Springer, 2022, pp. 18–35.
- [80] K. Yao, J. Wang, B. Diao, and C. Li, "Towards understanding the generalization of deepfake detectors from a game-theoretical view," in *IEEE/CVF Int. Conf. Comput. Vis.*, 2023, pp. 2031–2041.
- [81] L. S. Shapley, "A value for n-person games," *Annals of*

- Mathematics Studies*, pp. 307–317, 1953.
- [82] O. Russakovsky, J. Deng, H. Su, J. Krause, S. Satheesh, S. Ma, Z. Huang, A. Karpathy, A. Khosla, M. Bernstein *et al.*, “Imagenet large scale visual recognition challenge,” *Int. J. Comput. Vis.*, vol. 115, pp. 211–252, 2015.
- [83] C. Szegedy, W. Liu, Y. Jia, P. Sermanet, S. Reed, D. Anguelov, D. Erhan, V. Vanhoucke, and A. Rabinovich, “Going deeper with convolutions,” in *IEEE Conf. Comput. Vis. Pattern Recog.*, 2015, pp. 1–9.
- [84] K. Simonyan and A. Zisserman, “Very deep convolutional networks for large-scale image recognition,” *arXiv preprint arXiv:1409.1556*, 2014.
- [85] J. Hu, L. Shen, and G. Sun, “Squeeze-and-excitation networks,” in *IEEE/CVF Conf. Comput. Vis. Pattern Recog.*, 2018, pp. 7132–7141.
- [86] U. Ozbulak, H. J. Lee, B. Boga, E. T. Anzaku, H. min Park, A. V. Messem, W. D. Neve, and J. Vankerschaver, “Know your self-supervised learning: A survey on image-based generative and discriminative training,” *Mach. learn. res.*, 2023.
- [87] M. Caron, P. Bojanowski, A. Joulin, and M. Douze, “Deep clustering for unsupervised learning of visual features,” in *Eur. Conf. Comput. Vis.*, 2018, pp. 132–149.
- [88] W. Van Gansbeke, S. Vandenhende, S. Georgoulis, M. Proesmans, and L. Van Gool, “Scan: Learning to classify images without labels,” in *Eur. Conf. Comput. Vis.* Springer, 2020, pp. 268–285.
- [89] M. Caron, I. Misra, J. Mairal, P. Goyal, P. Bojanowski, and A. Joulin, “Unsupervised learning of visual features by contrasting cluster assignments,” *Adv. Neural Inf. Process. Syst.*, vol. 33, pp. 9912–9924, 2020.
- [90] X. Chen, H. Fan, R. Girshick, and K. He, “Improved baselines with momentum contrastive learning. arxiv 2020,” *arXiv preprint arXiv:2003.04297*, 2003.
- [91] X. Chen, S. Xie, and K. He, “An empirical study of training self-supervised vision transformers,” in *IEEE/CVF Int. Conf. Comput. Vis.*, 2021, pp. 9640–9649.
- [92] K. He, H. Fan, Y. Wu, S. Xie, and R. Girshick, “Momentum contrast for unsupervised visual representation learning,” in *IEEE/CVF Conf. Comput. Vis. Pattern Recog.*, 2020, pp. 9729–9738.
- [93] T. Chen, S. Kornblith, M. Norouzi, and G. Hinton, “A simple framework for contrastive learning of visual representations,” in *Int. Conf. Mach. Learn.* PMLR, 2020, pp. 1597–1607.
- [94] T. Chen, S. Kornblith, K. Swersky, M. Norouzi, and G. E. Hinton, “Big self-supervised models are strong semi-supervised learners,” *Adv. Neural Inf. Process. Syst.*, vol. 33, pp. 22 243–22 255, 2020.
- [95] J.-B. Grill, F. Strub, F. Altché, C. Tallec, P. Richemond, E. Buchatskaya, C. Doersch, B. Avila Pires, Z. Guo, M. Gheshlaghi Azar *et al.*, “Bootstrap your own latent—a new approach to self-supervised learning,” *Adv. Neural Inf. Process. Syst.*, vol. 33, pp. 21 271–21 284, 2020.
- [96] X. Chen and K. He, “Exploring simple siamese representation learning,” in *IEEE/CVF Conf. Comput. Vis. Pattern Recog.*, 2021, pp. 15 750–15 758.
- [97] M. Caron, H. Touvron, I. Misra, H. Jégou, J. Mairal, P. Bojanowski, and A. Joulin, “Emerging properties in self-supervised vision transformers,” in *IEEE/CVF Int. Conf. Comput. Vis.*, 2021.
- [98] A. Bardes, J. Ponce, and Y. LeCun, “Vicreg: Variance-invariance-covariance regularization for self-supervised learning,” *arXiv preprint arXiv:2105.04906*, 2021.
- [99] J. Devlin, M.-W. Chang, K. Lee, and K. Toutanova, “BERT: Pre-training of deep bidirectional transformers for language understanding,” *arXiv preprint arXiv:1810.04805*, 2018.
- [100] H. Bao, L. Dong, S. Piao, and F. Wei, “Beit: Bert pre-training of image transformers,” *arXiv preprint arXiv:2106.08254*, 2021.
- [101] X. Chen, M. Ding, X. Wang, Y. Xin, S. Mo, Y. Wang, S. Han, P. Luo, G. Zeng, and J. Wang, “Context autoencoder for self-supervised representation learning,” *Int. J. Comput. Vis.*, vol. 132, no. 1, pp. 208–223, 2024.
- [102] K. Yi, Y. Ge, X. Li, S. Yang, D. Li, J. Wu, Y. Shan, and X. Qie, “Masked image modeling with denoising contrast,” *Int. Conf. Learn. Represent.*, 2023.
- [103] Z. Liu, P. Luo, X. Wang, and X. Tang, “Deep learning face attributes in the wild,” in *IEEE Int. Conf. Comput. Vis.*, 2015.
- [104] T. Karras, S. Laine, and T. Aila, “A style-based generator architecture for generative adversarial networks,” in *IEEE/CVF Conf. Comput. Vis. Pattern Recog.*, 2019, pp. 4401–4410.
- [105] M. Sensoy, L. Kaplan, and M. Kandemir, “Evidential deep learning to quantify classification uncertainty,” *Adv. Neural Inf. Process. Syst.*, vol. 31, 2018.
- [106] W. Bao, Q. Yu, and Y. Kong, “Evidential deep learning for open set action recognition,” in *IEEE/CVF Int. Conf. Comput. Vis.*, 2021, pp. 13 349–13 358.
- [107] A. Jsang, *Subjective Logic: A formalism for reasoning under uncertainty*. Springer Publishing Company, Incorporated, 2018.
- [108] T. Fawcett, “An introduction to roc analysis,” *Pattern recognition letters*, vol. 27, no. 8, pp. 861–874, 2006.
- [109] D. M. Powers, “Evaluation: from precision, recall and f-measure to roc, informedness, markedness and correlation,” *arXiv preprint arXiv:2010.16061*, 2020.
- [110] J. Yu, H. Zhu, L. Jiang, C. C. Loy, W. Cai, and W. Wu, “CelebV-Text: A large-scale facial text-video dataset,” in *IEEE/CVF Conf. Comput. Vis. Pattern Recog.*, 2023.
- [111] “Deepfakes github,” 2018. [Online]. Available: <https://github.com/deepfakes/faceswap>
- [112] M. Kowalski, “Faceswap github,” 2020. [Online]. Available: <https://github.com/MarekKowalski/FaceSwap>
- [113] J. Thies, M. Zollhofer, M. Stamminger, C. Theobalt, and M. Nießner, “Face2face: Real-time face capture and reenactment of rgb videos,” in *IEEE Conf. Comput. Vis. Pattern Recog.*, 2016, pp. 2387–2395.
- [114] J. Thies, M. Zollhöfer, and M. Nießner, “Deferred neural rendering: Image synthesis using neural textures,” *ACM Trans. Graph.*, vol. 38, no. 4, pp. 1–12, 2019.
- [115] T. Zhou, W. Wang, Z. Liang, and J. Shen, “Face forensics in the wild,” in *IEEE/CVF Conf. Comput. Vis. Pattern Recog.*, 2021, pp. 5778–5788.
- [116] A. Radford, “Unsupervised representation learning with deep convolutional generative adversarial net-

- works," *arXiv preprint arXiv:1511.06434*, 2015.
- [117] T. Xu, P. Zhang, Q. Huang, H. Zhang, Z. Gan, X. Huang, and X. He, "Attngan: Fine-grained text to image generation with attentional generative adversarial networks," in *IEEE/CVF Conf. Comput. Vis. Pattern Recog.*, 2018, pp. 1316–1324.
- [118] R. Rombach, A. Blattmann, D. Lorenz, P. Esser, and B. Ommer, "High-resolution image synthesis with latent diffusion models," in *IEEE/CVF Conf. Comput. Vis. Pattern Recog.*, 2022, pp. 10 684–10 695.
- [119] K. Kim, Y. Kim, S. Cho, J. Seo, J. Nam, K. Lee, S. Kim, and K. Lee, "Diffface: Diffusion-based face swapping with facial guidance," *arXiv preprint arXiv:2212.13344*, 2022.
- [120] M. Stypułkowski, K. Vougioukas, S. He, M. Zięba, S. Petridis, and M. Pantic, "Diffused heads: Diffusion models beat gans on talking-face generation," in *IEEE/CVF Conf. Comput. Vis. Pattern Recognit. Workshops*, 2024, pp. 5091–5100.
- [121] J. Deng, J. Guo, Y. Zhou, J. Yu, I. Kotsia, and S. Zafeiriou, "Retinaface: Single-stage dense face localisation in the wild," *arXiv preprint arXiv:1905.00641*, 2019.
- [122] Y. You, J. Li, S. Reddi, J. Hseu, S. Kumar, S. Bhojanapalli, X. Song, J. Demmel, K. Keutzer, and C.-J. Hsieh, "Large batch optimization for deep learning: Training bert in 76 minutes," *arXiv preprint arXiv:1904.00962*, 2019.
- [123] S. Gidaris, A. Bursuc, G. Puy, N. Komodakis, M. Cord, and P. Pérez, "Obow: Online bag-of-visual-words generation for self-supervised learning," in *IEEE/CVF Conf. Comput. Vis. Pattern Recog.*, 2021, pp. 6830–6840.
- [124] Z. Wang, Y. Guo, and W. Zuo, "Deepfake forensics via an adversarial game," *IEEE Trans. Image Process.*, vol. 31, pp. 3541–3552, 2022.
- [125] L. Van der Maaten and G. Hinton, "Visualizing data using t-sne." *JMLR*, vol. 9, no. 11, 2008.
- [126] Y. Guo, L. Zhang, Y. Hu, X. He, and J. Gao, "Ms-celeb1m: Challenge of recognizing one million celebrities in the real world," *Electronic imaging*, vol. 28, pp. 1–6, 2016.
- [127] D. Miller, E. Brossard, S. Seitz, and I. Kemelmacher-Shlizerman, "Megaface: A million faces for recognition at scale," *arXiv preprint arXiv:1505.02108*, 2015.
- [128] Y. Zheng, H. Yang, T. Zhang, J. Bao, D. Chen, Y. Huang, L. Yuan, D. Chen, M. Zeng, and F. Wen, "General facial representation learning in a visual-linguistic manner," in *IEEE/CVF Conf. Comput. Vis. Pattern Recog.*, 2022, pp. 18 697–18 709.
- [129] B. M. Le and S. S. Woo, "Gradient alignment for cross-domain face anti-spoofing," in *IEEE/CVF Conf. Comput. Vis. Pattern Recog.*, 2024.
- [130] Z. Boulkenafet, J. Komulainen, L. Li, X. Feng, and A. Hadid, "Oulu-npu: A mobile face presentation attack database with real-world variations," in *2017 12th IEEE international conference on automatic face & gesture recognition (FG 2017)*. IEEE, 2017, pp. 612–618.
- [131] Z. Zhang, J. Yan, S. Liu, Z. Lei, D. Yi, and S. Z. Li, "A face antispoofing database with diverse attacks," in *2012 5th IAPR international conference on Biometrics (ICB)*. IEEE, 2012, pp. 26–31.

- [132] I. Chingovska, A. Anjos, and S. Marcel, "On the effectiveness of local binary patterns in face anti-spoofing," in *2012 BIOSIG-proceedings of the international conference of biometrics special interest group (BIOSIG)*. IEEE, 2012, pp. 1–7.
- [133] D. Wen, H. Han, and A. K. Jain, "Face spoof detection with image distortion analysis," *IEEE Trans. Inf. Forensics Security.*, vol. 10, no. 4, pp. 746–761, 2015.



image/video

Zonghui Guo (Member, IEEE) received Ph.D. degree in intelligence information and communication systems from the Ocean University of China, Qingdao, China, in 2021. He is currently a Postdoctoral Researcher with the Institute of Computing Technology (ICT), Chinese Academy of Sciences (CAS), Beijing, China. His research interests include face forgery detection, low-level vision applications such as harmonization, and image/video enhancement.



Yingjie Liu (Student Member, IEEE) received the B.E. degree in information engineering from the Qingdao University of Science and Technology, Qingdao, China, in 2022. He is currently a Postgraduate Student with the College of Electronic Engineering, Ocean University of China, Qingdao, China. His research interests include face forgery detection and presentation attack detection.



supervised learning, domain generalization.

Jie Zhang (Member, IEEE) is an associate professor with the Institute of Computing Technology, Chinese Academy of Sciences (CAS). He received the Ph.D. degree from the University of Chinese Academy of Sciences, Beijing, China. His research interests cover computer vision, pattern recognition, machine learning, particularly include face recognition, image segmentation, weakly/semi-supervised learning, domain generalization.



computer vision, underwater vision, and deep learning.

Haiyong Zheng (Senior Member, IEEE) received the B.E. degree in electronic information engineering and the Ph.D. degree in ocean information sensing and processing from the Ocean University of China, Qingdao, China, in 2004 and 2009, respectively. In 2009, he joined the College of Electronic Engineering, Ocean University of China, where he is currently a Professor. His research interests include computer vision, underwater vision, and deep learning.



machine learning.

Shiguang Shan (Fellow, IEEE) received Ph.D. degree in computer science from the Institute of Computing Technology (ICT), Chinese Academy of Sciences (CAS), Beijing, China, in 2004. He has been a full professor of this institute since 2010 and now the director of CAS Key Lab of Intelligent Information Processing. His research interests cover computer vision, pattern recognition, and machine learning. He has published more than 300 papers, with totally more than 38,000 Google scholar citations. He has served as Area Chair (or Senior PC) for many international conferences including ICCV11, ICPR12/14/20, ACCV12/16/18, FG13/18, ICASSP14, BTAS18, AAAI20/21, IJCAI21, and CVPR19/20/21. And he was/is Associate Editors of several journals including IEEE T-IP, Neurocomputing, CVIU, and PRL. He was a recipient of the China's State Natural Science Award in 2015, and the China's State S&T Progress Award in 2005 for his research work.